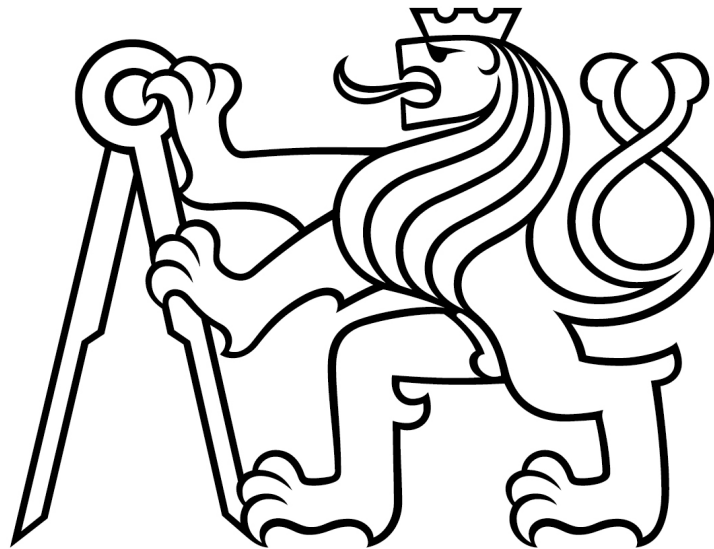# CONCEPTUAL DESIGN OF A HYBRID ROCKET ENGINE FOR A ROCKET TO EXPLORE THE MESOSPHERE

FACULTY OF MECHANICAL ENGINEERING

MASTER THESIS

Ivan Šonka

ÚSTAV LETADLOVÉ A KOSMICKÉ TECHNIKY
CZECH TECHNICAL UNIVERSITY IN PRAGUE
Prague, 2021

ZADÁNÍ DIPLOMOVÉ PRÁCE

I. OSOBNÍ A STUDIJNÍ ÚDAJE

Příjmení: **Šonka**   Jméno: **Ivan**   Osobní číslo: **437750**

Fakulta/ústav: **Fakulta strojní**

Zadávající katedra/ústav: **Ústav letadlové techniky**

Studijní program: **Letectví a kosmonautika**

Studijní obor: **Letadlová a kosmická technika**

II. ÚDAJE K DIPLOMOVÉ PRÁCI

Název diplomové práce:

Koncepční návrh hybridního raketového motoru pro nosič k průzkumu mezosféry

Název diplomové práce anglicky:

Conceptual design of a hybrid engine for a rocket to explore the mesosphere

Pokyny pro vypracování:

Pro vypracování proveďte:
- Rešerši hybridních raketových motorů
- Ideový návrh motoru
- Konstrukční návrh jednotlivých konstrukčních celků (tryska, spalovací komora, zapalování, injektor okysličovadla, systém dopravy okysličovadla)
- Ideový návrh testovacího standu

Seznam doporučené literatury:

Jméno a pracoviště vedoucí(ho) diplomové práce:

Ing. Jaromír Kučera,   ústav letadlové techniky   FS

Jméno a pracoviště druhé(ho) vedoucí(ho) nebo konzultanta(ky) diplomové práce:

Datum zadání diplomové práce: **30.04.2021**   Termín odevzdání diplomové práce: **30.07.2021**

Platnost zadání diplomové práce: _____

_____
Ing. Jaromír Kučera
podpis vedoucí(ho) práce

_____
Ing. Robert Theiner, Ph.D.
podpis vedoucí(ho) ústavu/katedry

_____
prof. Ing. Michael Valášek, DrSc.
podpis děkana(ky)

III. PŘEVZETÍ ZADÁNÍ

_____
.
Datum převzetí zadání

_____
Podpis studenta

Declaration

I declare that I have developed and written this Master thesis completely by myself, under guidance of thesis supervisor Ing. Jaromír Kučera. All sources used are declared in the list of literature.

....

Acknowledgement

I would like to thank to Ing. Jaromír Kučera for his guidance, his advice and his willingness to consult even at the last minute and also for his patience. My gratitude is also towards my family, especially my brother for pointing out my mistakes.

Anotační list

Jméno autora:

Bc. Ivan Šonka

Název DP:

Koncepční návrh hybridního raketového motoru pro nosič k průzkumu mezosféry

Anglický název:

Conceptual Design of a hybrid rocket engine for a rocket to explore the mesosphere

Akademický rok:

2020/2021

Ústav:

Ústav letadlové techniky

Vedoucí DP:

Ing. Jaromír Kučera

Klíčová slova: Hybridní raketový motor, Tryska, Okysličovadlo, Hybridní spalování

Keywords: Hybrid rocket engine, Nozzle, Oxidizer, Hybrid combustion

Anotace Tato diplomová práce je zaměřena na koncepční návrh hybridního raketového motoru pro nosič k průzkumu mezosféry. Dle rešerže s důrazem na hybridní sondážní rakety byla vybrána kombinace okysličovadla a pevného paliva. Pro tuto kombinace byly početně navrženy subsystémy tryska, přívod a vstřikování okysličovadla, zapalování, spalovací komora a chlazení na koncepční úrovni. Dále byl ideologicky naržen testovací stand pro motor.

Abstract: The scope of this thesis is to perform conceptual design of the hybrid rocket engine for a rocket able to reach mesosphere. Based on the theoretical research with greater emphasis on the utilization of the hybrid propulsion with the sounding rockets I have decide the suitable propellant combination. Performed feasibility study to determine the suitable length of the burn time and propellant masses. Based on the data found I have designed the individual subsystems of the rocket, nozzle, combustion chamber, oxidizer supply and injection, ignition system and cooling system to a conceptual level. I also presented ideological design for test stand for the engine. Certain subsystems offer opportunity to be assessed in greater depth with possible optimizations.

Contents

List of Figures

List of Tables

Nomenclature

Subscripts

1	At nozzle inlet
2	At nozzle exit
a	Ambient
b	Burn
c	Combustion
$cone$	For conical nozzle
cyl	Pressurant
ext	External
f	Fuel
g	Gas 3.7.1
g	Grain
i	Internal
l	Liquid
or	Orifice
out	At the end of burn
ox	Oxidizer
pas	Passage
$peak$	At the peak altitude
pr	Cylidrical
$prop$	Propellant
t	At nozzle throat
tot	Total
u	Ullage

w wall

Symbols

$\dot{m}$ Mass flow (kg/s)

$\dot{Q}$ Volume flow ($\mathrm{m^3}/s$)

$\dot{r}$ Regression rate (mm/s)

ϵ Area ratio

γ Specific heat ratio

λ Correction factor

μ Dynamic viscosity (Pa·s)

ρ Density ($\mathrm{kg/m^3}$)

σ Yield stress (MPa)

A Area ($\mathrm{m^2}$)

a Acceleration (m/s^2)

c^* Characteristic velocity (m/s)

C_D Drag coefficient

C_d Discharge coefficient

C_p Specific at constant pressure (J/kgK)

C_v Specific at constant volume (J/kgK)

C_{d0} Zero-lift drag coefficient

d Diameter (m)

F Force (N)

G Local mass flux ($\mathrm{kg/m^2}s$)

h Enthalpy (J)

h Film coefficient ($\mathrm{W/m^2}K \cdot s$)

h Height (m)

I_{SP} Specific impulse (Ns/kg)

k Thermal conductivity (W/m·K)

L Length (m)

M Mach number, except for 3.60, in this case Molar mass (g/mol)

m Mass (kg)

n Number of moles (mol)

O/F Oxidizer to fuel ratio (-)

p Pressure (Pa)

R Molar gas constant (J/molK)

r Radius (m)

R^* Specific molar gas constant (J/kgK)

T Thermodynamic temperature (K)

T Thrust (N)

t Thickness (m)

t Time (s)

u Gas flow velocity (m/s)

V Volume (m^3)

W Weight (N)

1. Introduction

A hybrid rocket engine utilizes propellants which are stored in different phases. Even though there are some hybrid engines employing liquid fuel and solid oxidizer, the most common, classical hybrid, uses liquid oxidizer and solid fuel grain.

Hybrid rocket engines hold both advantages and disadvantages over the other two types of engines, solids and liquids. These will be discussed later on in this thesis, but the advantages make hybrid rocket engines attractive especially for academic purposes and also for certain types of commercial uses.

The scope of this thesis is to create a conceptual design of a hybrid rocket engine for a sounding rocket able to perform measurements in the mesosphere. The goal is to provide baseline design for combustion chamber, nozzle, oxidizer feeding system and other crucial engine elements, which can developed further in years to come.

2. Hybrid Rocket Engines

In this chapter the history of hybrid rocket engines is briefly discussed. The basic principles of hybrid engine rocketry, advantages and disadvantages compared to solid and liquid engines along with potential applications for vehicles with hybrid rocket propulsion. Followed by a summarization of the combustion principles and regression rate. Finally possible and popular combinations of the propellants are listed, with comparison of I_{SP} developed by the specific combinations.

2.1 History of hybrid rocket engines

First successful recorded use of the hybrid rocket engine dates to the year 1933, when researchers from Soviet Group of the Study of Reactive Motion (GIRD) launched GIRD-9. This engine used gelled gasoline and liquid oxygen as propellants. On the first attempt the vehicle reached altitude of 400 meters, on the second attempt in 1934 the GIRD-9 rocket reached 1500 meters.

In the late 1930s Germans initiated efforts of their own in the hybrid rocket engine investigation. Their 10-kN hybrid engine used coal as the solid fuel grain and gaseous nitrous oxide as oxidizer. Carbon has a very high heat of sublimation, this causes poor burning rate and these experiments were not successful.

Beginning in the mid-1940s Pacific Rocket Society made noticeable effort in hybrid rocketry with the series of XDF engines. Over time the fuel grain evolved, from wood in the earlier attempts to rubber-based fuel in the latter. Early attempts experienced failures during the tests, XDF-3 used a wooden nozzle, even though it was soaked in a chloride solution it was demolished during operation, XDF-4 broke away from the test stand after 2 s of operation. Eventually XDF-23 made a

successful flight in 1951 and reached altitude of approximately 10 km.

In 1960s French launched their first hybrid rocket LEX, able to reach 100 km. In the late 60s Sweden introduced sounding hybrid rocket able to carry 20 kg of payload to 80 km.

Major breakthrough for hybrid rocket engines came in 1984, when company Starstruck Inc. developed and launched Dolphin sounding rocket. This sea-launched vehicle was first privately developed and first large scale hybrid. Weighing 7,500 kg and able to develop up to 155 kN of thrust. These attempts to privately engineer hybrid rocket engines were soon followed by another American Rocket Company (AMROC), with over 300 hybrid engines test. Tested engines range from 4.5 kN up to 1.1 MN of thrust. In the 1996 the company was shut down, but 4 years later their intellectual property was taken on by SpaceDev and some of it was used in development of SpaceShipOne.

NASA joined hybrid rocket endeavour in 1995 with Hybrid Propulsion Demonstration Program. Several Hyperion rockets built under this program utilized combination of HTPB and N_2O.

One of the most recent vehicles utilizing hybrid rocket engines is the Virgin Galactic's SpaceShipOne and SpaceShipTwo. Primary goal of this program is to provide space tourism opportunities. Both vehicles were designed for air-launch by a mother ship, approximately at the altitude of 15 km, for the SpaceShipTwo, the latter and more recent iteration, the engine is ignited afterwards with a burn time of 70 seconds. After the engine powered flight the vehicle is to coast beyond the Karmán line, approximately 110 km. SpaceShipOne used $HTPB/N_2O$ as a propellant, for SpaceShipTwo new engine was developed, simply called RocketMotorTwo, during the development it was considered to change the combination to polyamid plastic as the fuel grain, but eventually company came back to the original combination. RocketMotorTwo develops 310 kN of thrust with a specific impulse of 250 s (2,452.5 Ns/kg).

2.2 Basic principles of hybrid rocketry

As it was mentioned in the introduction the crucial feature of the hybrid engine that distinguishes it from solid and liquid engines is the fact, that oxidizer and propellant are kept in separate phases. Most common is the combination of solid fuel grain and liquid oxidizer. Reversed hybrid engines use the opposite combination. Unlike the liquid engines, where oxidizer and propellant are mixed with the desired O/F ration in the combustion chamber and ignited, the hybrid engine has a solid fuel grain likely in a form of a tube. Oxidizer is then pressure fed via a valve and an injector, as it can be seen in the schematics 2.1. One the major differences between liquid and hybrid engine is the shift of O/F ration, in the combustion chamber of liquid rocket engine O/F remains the same, for the hybrid engine combustion chamber the O/F shifts as we travel along the length of the fuel grain. Another major factor influencing the overall performance of the hybrid engine is the cross section of the chosen fuel grain. For the solid engines the cross section of the propellant grain determines the shape of the thrust over time curve. This effect is similar with the hybrid engines, nevertheless hybrid engines have crucial advantage, they usually have the possibility to reduce or increase the mass flow of the oxidizer and throttle the engine.
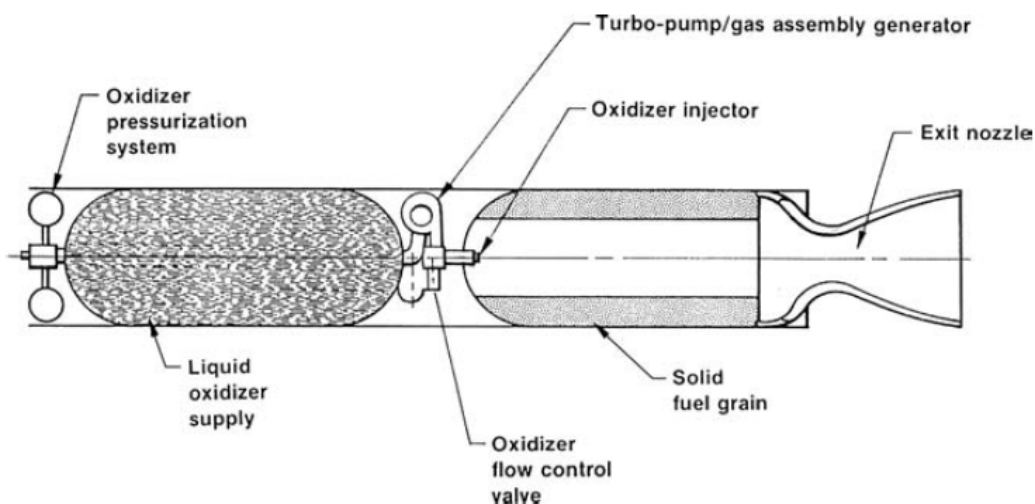
Figure 2.1: Hybrid rocket schematics

4

2.2.1 Advantages and disadvantages

There are several key aspects, when it comes to propulsion engineering and rocket engine features such as performance, simplicity, reliability, safety of operations, design and operations costs and in recent years environmental impact has also become a topic that needs to be addressed. The nature of the hybrid rocket engines affords certain advantages over the liquids and solids, yet it also has certain disadvantages.

Advantages over liquids

- **Mechanical simplicity** - With only either oxidizer or fuel in the liquid phase, the hybrid rocket engine system requires less complex overall construction, resulting in less plumbing, less valves, less pressurized vessels and pumping features.

- **Higher propellant density** - Fuel grain in the solid phase usually has higher density compared to liquid fuels. thus reducing overall volume and construction costs and weight of the system. However with bigger combustion chambers it is necessary to use fuel grain with multiple ports, as the area of the fuel grain exposed to the flame must increase. This lowers the overall bulk density of the solid propellant and mitigates this advantage.

- **Propellant versatility** - There are many different oxidizer/fuel combinations to use. Some of these being hypergolic. To further increase the performance additives can be added to the fuel grain, materials like aluminium, magnesium, lithium and others. Although this has also negative side effect. Small particles of the metal additives might be propelled into the nozzle after combustion. These small particles with high velocity have abrasive effect on the nozzle and one must take this effect into account when using additives.

- **Simplified throttling** - The engine can be throttled by altering the flow of the liquid phase, therefore it is not necessary to match the flow of both oxidizer

and fuel, which must be synchronized for the liquid engines. The flow of the solid propellant alters due to reduction or increase in the liquid flow. Shut down of the engine can be achieved by simply terminating the liquid flow.

- **Safety** - Safety is of paramount importance when it comes to propulsion system engineering. As the solid fuel polymers are usually used. "The fuel is inert and can be manufactured, transported, and handled safely in accordance with standard commercial practice. The system is nonexplosive because an intimate mixture of oxidizer and fuel is not possible"

Advantages over solids

- **Able to restart and throttle** - Once the solid engine is ignited it is impossible to shut it down and restart. Hybrid engine equipped with igniter or hypergolic propellant combination can be shut down and restarted. Reducing the liquid flow can be used to throttle the engine, this is not possible with the solid engines. The solid part of the propellant responds accordingly to the flow of the liquid. The greatest influence one can have on the thrust development over time in the solid engine is by the choice of the fuel grain cross section.

- **Higher performance** - Hybrid engines have higher theoretical specific impulse I_{SP}.

- **Safety** Hybrid engines have reduced hazards during the propellant transportation, solid and liquid phase can be transported separately. As the substances used in solid propellant are often chemically incompatible, solid fuel grain can suffer defects and distortions. Fuel grain faults can be also found in the hybrid rocket engine, but they are less likely to occur and usually are developed during the manufacturing process and are stable when stored.

- **Easier fuel preparation** - As mentioned above the process of preparing solid fuel grain poses explosion hazards and uses harmful chemical substances. For hybrid rocket engines polymer based fuel grains can be used, which are safe to handle.

Disadvantages of the hybrids

- **Regression rate** - Fuel grain regression rate is closely tied to the thrust and performance of the engine. For bigger combustion chambers the fuel grain needs to have multiple ports in order to develop sufficient thrust. "...most combustion chambers over a foot in diameter require multiple ports to provide adequate burning surface to meet the required thrust. This characteristic, however, is desirable for long-duration applications with a low-thrust requirement such as target drones, hovering vehicles..."

- **Combustion efficiency** - Hybrids usually have lower combustion efficiency compared to both solids and liquids due to the large diffusion flame, which results in lower mixing rate. Nevertheless hybrids have higher theoretical specific impulse I_{SP}, this results in hybrid vehicle being able to outperform solid in the end.

- **O/F shift** - With longer burn times the initial port size increases as the larger surface area is exposed to the flame. The second cause of the O/F shift is the change due to the combustion, making the O/F ratio shift along the length of the port. With proper initial O/F design these can be reduced and held at less then 1%.

- **Throttle response rate** - Speed of the response to the change of the liquid flow is lower compared to liquid engines. Hybrid engines are therefore viable for the applications, where speed of the response is not of a paramount importance.

2.2.2   Potential applications

Generally the hybrid rocket engines can be used in every rocket applications, due to the advantages and disadvantages discussed above there are some applications where they are superior to the competition.

- **Sounding rockets** - This is probably the most extensive use of hybrid rocket engines. Various widely accessible propellants make the hybrid engine desirable for sounding rockets. Generally sounding rockets have low cost and short lead time, with their use being typically meteorology and upper atmosphere research. Compared to weather balloons and satellites they can reach altitudes inaccessible to these. Sometimes they can also be used to test and experiment on technology meant to be used in orbital programs. As it was discussed in the 2 some of the early experiments with the hybrid rocketry were sounding rockets.

- **Space engines** - Ability to shut down and restart and to throttle the engine during the run combined with the not so complex construction make hybrid engines viable also for providing the exact final velocity to guide vehicle on it's orbit.

- **Boosters** - The ability to provide large amounts of thrust makes hybrids also desirable as the boosters for larger vehicles. Throttling and shut down/restart feature are major advantages over the solid boosters, increasing the safety of operations of the vehicle. "The incentive for this development was to provide a throttling and thrust termination capability for both vehicle performance improvement and abort capability in the event of a system failure. This interest was partially stimulated by the Space Shuttle Challenger failure in 1986." [10]

2.3 Hybrid engine combustion

To initiate hybrid engine combustion it is first necessary to vaporize the solid fuel. By providing the source of heat, from the igniter, the fuel grain surface vaporizes. Through the injector oxidizer is fed into the combustion chamber and mixes with the vaporized fuel particles. If enough of the fuel grain has been vaporized the mix becomes combustible and engine is ignited. After the ignition fuel grain surface pyrolyzes due to the heat of the flame, which is formed at approximately

10-20% of the boundary layer thickness above the surface. Pyrolyzed fuel moves into the flame zone and reacts with the gasseous oxidizer, resulting in more heat to sustain pyrolysis. "The fuel mass flux due to pyrolysis, however, blocks some of the heat transfer to the surface, which causes a decrease in the regression rate and corresponding strength of the wall blowing effect and, in turn, a weakening of the blocking action, which in turns means that more heat can reach the surface, and so on. This tendency toward a self-regulating interaction between heat flux, mass blowing, and heat flux blockage is a distinguishing characteristic of hybrid combustion." [10]
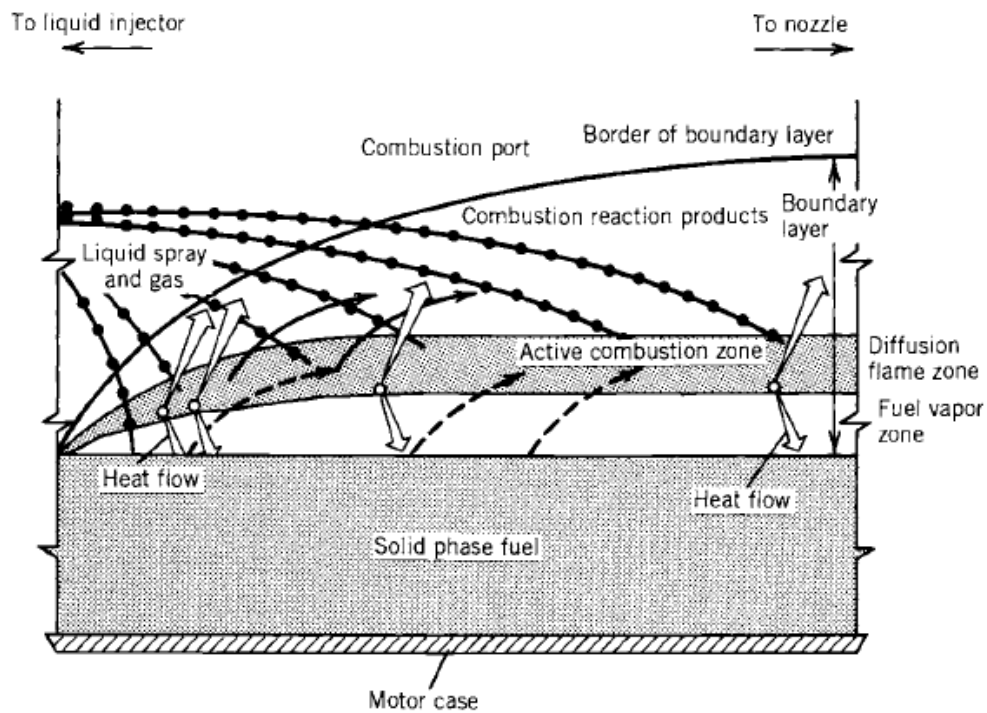

Figure 2.2: Simplified model of the hybrid combustion [3]

Below the active combustion zone a fuel rich zone is formed, in a similar fashion above the combustion zone a oxidizer rich zone forms. The oxidizer under specific conditions may be able to pass through the flame zone and interact with the fuel on the pyrolyzing surface.

2.3.1 Regression rate

One of the key factors of the hybrid engine is the regression rate, which depicts how fast the fuel surface recedes over time of the operation. Based on the values of the regression rate the fuel grain dimensions are determined, therefore it has first order impact upon the design of the engine, it directly effects the combustion chamber length and diameter. Accurate data are also crucial for the design in order to avoid premature burn out or on the other hand residual unburned fuel grain adding mass burden to the rocket.

One of the earliest analysis of the regression rate is shown in the 2.1, adapted from [11]. This theory was models the hybrid combustion as a diffusion flame with a turbulent boundary layer, formed above the pyrolyzing surface. This model also takes in account the effect of the "heat blocking effect" of the fuel mass transferring into the boundary layer.

$$\dot{r} = \frac{0.036G}{\rho_f} \left(\frac{Gx}{\mu} \right)^{-0.2} \left(\frac{u_e \triangle h}{u_c h_v} \right) \tag{2.1}$$

The instantaneous local regression rate $\dot{r}$, instantaneous local mass flux G and the distance along the port length x are the variables of the equation, while the velocity ratio, ratio of enthalpy difference and main steam viscosity are constants. The coefficient 0.036 if for imperial units, for which the expression was originally derived.

Over the years tests results proved the validity of the Marxman's regression rate law, but the common practice for regression rate analysis is to utilize a form of reggresion rate law augumented by exponents and coefficients, empirically found from subscale experiments.

$$\dot{r} = a G_{ox}^n x^m \tag{2.2}$$

Exponents n and m and the coefficient a are determined experimentally, the coefficient a is not a unit less coefficient, therefore care for usage of consistent

units must be taken. Another advantage the second expression for regression rate holds is the usage of oxidizer mass flux G_{ox}, much more easily measurable quantity, compared to the overall mass flux. [13]

2.4 Propellant combinations

The classical hybrid, liquid oxidizer and solid fuel, has a wide inventory of available propellant combination. Choice is more restricted for the reverse hybrid, because the solid oxidizers are in limited number and it is difficult to use in larger scales, due to the mechanical limitations.

Probably the most popular among the solid fuel grains is the HTPB (Hydroxyl-terminated polybutadiene), other polybutadiene based polymers are also suitable, but the HTPB is generally the favourite of this group, due to commercial availability. Other hydrocarbons can be used, to name a few: paraffin wax, polyethylen even coal and wood, which were used in earlier days. One of the advantages of these polymer fuels is the possibility of introducing performance additives, such as $Al, AlH_3, Li, LiH, LiAlH_4$ etc. "These additives can enhance either motor performance through Isp improvement or vehicle performance through increased density and, hence, mass fraction." [10].

Special type of the solid fuel grains are the cryogenic solids, gasses like pentane, methane, carbon oxide, oxygen and hydrogen are frozen solid and used as the fuel grain. The goal in development of this solids was to come up with a hybrid combination able to compete with the high-performance liquid cryogenic propellants. The technological challenges that arise with the use of cryogenic solids, the added weight of the required insulation, inconvenient manipulation and generally larger expanses overshadow the advantages.

For the liquid oxidizers essentially the substances as with the liquid engines are used. Chiefly being the O_2 and FLOX (2 part F_2 to 1 part O_2 mixture. N_2O is also very popular for smaller scale engines, because it is widely available in a form of charges for cream whippers. For the solid oxidizers we can name nitronium

Fuel	Oxidizer	Optimum O/F	Sea level I_sp (Ns/kg)	c^* (m/s)
HTPB	LOX	1.9	2 745	1 820
HTPB	N_2O	7.1	2 423	1 604
HTPB	FLOX	3.3	3 080	2 042
PE	LOX	2.5	2 737	1 791
PE	N_2O	8.0	2 423	1 600
Paraffin	LOX	2.5	2 756	1 804
Paraffin	N_2O	8.0	2 432	1 606
HTPB/Al(40%)	LOX	1.1	2 687	1 757
HTPB/Al(40%)	N_2O	3.5	2 472	1 637
Carbon	LOX	1.9	2 443	1 599
Carbon	N_2O	6.3	2 315	1 522
Cryogenic hybrids				
Pentane	LOX	2.7	2 737	1 761
CH_4	LOX	3.0	2 855	1 871
Reverse hybrids				
JP-4	AP	9.1	2 305	1 526
JP-4	NP	3.6	2 541	1 669

Table 2.1: Table with several chosen fuel/oxidizer combinations and their performance factors, $p_c = 3.45MPa$ $p_a = 0.1MPa$, adapted from [10], originally listed imperial units were converted into metric

perchlorate and ammonium perchlorate, which were used in combination with JP-4 (Jet Propellant), 50-50 blend of kerosine and gasoline. The combinations with solid oxidizers are low performing, NP, being the stronger oxidizer, can be hypergolic in contact with organic materials and AP is generally unstable so both have explosive danger. Longer exposure to perchlorates also results in various thyroid related health issues.

2.4.1 Propellant choice

Based on the information found in the table 2.1 to use classical hybrid with a paraffin/LOX propellant combination. In the initial preliminary analysis the combination of HTPB/LOX was also considered, but paraffin is more affordable and easier to reform into the desired fuel grain shape.

3. Hybrid Rocket Engine Design

     In this chapter the conceptual design itself is discussed. First there is a feasibility study and preliminary design, where the ideal burn time for the engine in order to reach upper stages of atmosphere is decided. Followed by a design of sub-systems of the engine, nozzle, combustion chamber, ignition, oxidizer injector and supply system.

3.1 Preliminary Propellant Design

     First thing to address in this chapter is the preliminary design of the oxidizer and fuel grain. We aimed to get preliminary values of the mass flow, mass and volume for the chosen propellant combination in order to perform feasibility analysis in later section in order to evaluate the engine suitability for the desired application.

     As the propellant combination of liquid oxygen and paraffin wax were chosen. Three different burn times were considered 30, 45, 60 seconds. As the input data for the preliminary calculations of propellant masses, flows and volumes have served the ideal O/F, I_{SP} and T.

I_{SP}	T	O/F
2 756.61	15 000	2.5

Table 3.1: Input values for the preliminary calculation

     Using following equations we have calculated the propellant mass flow, oxidizer mass flow, fuel mass flow. The values substituted into the listed expressions are for the burn time $t_b = 45s$, which was later in the section 3.2 deemed as the most viable setup.

$$\dot{m}_{prop} = \frac{T}{I_{SP}} \tag{3.1}$$

$$\dot{m}_{prop} = \frac{15\,000}{2\,756.61} = 5.44 \tag{3.2}$$

$$\dot{m}_f = \frac{\dot{m}_{prop}}{1 + \frac{O}{F}} \tag{3.3}$$

$$\dot{m}_f = \frac{5.44}{1 + 2.5} = 1.55 \tag{3.4}$$

$$\dot{m}_{ox} = \dot{m}_{prop} - \dot{m}_f \tag{3.5}$$

$$\dot{m}_{ox} = 5.44 - 1.55 = 3.89 \tag{3.6}$$

Based on the burn time t_b we have calculated the needed mass of the propellant needed, followed by the oxidizer and the fuel masses:

$$t_b = \frac{m_{prop}}{\dot{m}_{prop}} \tag{3.7}$$

$$m_{prop} = t_b \cdot \dot{m}_{prop} \tag{3.8}$$

$$m_{prop} = 45 \cdot 5.44 = 244.87 \tag{3.9}$$

$$m_{ox} = \frac{m_{prop} \cdot \frac{O}{F}}{1 + \frac{O}{F}} \tag{3.10}$$

$$m_{ox} = \frac{244.87 \cdot 2.5}{1 + 2.5} = 174.9 \tag{3.11}$$

$$m_f = \frac{m_{prop}}{1 + \frac{O}{F}} \tag{3.12}$$

$$m_f = \frac{244.87}{1 + 2.5} = 69.96 \tag{3.13}$$

To determine volumes of the oxidizer and the fuel needed we must find the densities of the substances. We have assumed the liquid oxygen ρ_{OX}=1 281.2 kg/m^3 (at p=3 MPa and T=61 K) and the paraffin wax ρ_f=923 kg/m^3 (at p=1 atm and T=298 K). The found results are summarized in the table 3.2.

$$V_{ox} = \frac{m_{ox}}{\rho_{ox}} \tag{3.14}$$

$$V_{ox} = \frac{174.9}{1\,281.2} = 0.136 \tag{3.15}$$

$$V_f = \frac{m_f}{\rho_f} \tag{3.16}$$

$$V_f = \frac{69.96}{923} = 0.076 \tag{3.17}$$

t_b(s)	30	45	60
$\dot{m}_{prop}$ (kg/s)	5.44	5.44	5.44
$\dot{m}_f$ (kg/s)	1.55	1.55	1.55
$\dot{m}_{ox}$ (kg/s)	3.89	3.89	3.89
m_{prop}(kg)	163.24	244.87	326.49
m_{ox}(kg)	116.6	174.9	233.21
m_f(kg)	46.64	69.96	93.28
V_{ox}(m^3)	0.091	0.136	0.182
V_f(m^3)	0.051	0.076	0.101

Table 3.2: Summarization of the propellant design

3.2 Feasibility Analysis

With the chosen propellant combination, paraffin wax as the solid fuel and liquid oxygen as the oxidizer, it is necessary to decide the burn time of the engine. Three different variants were on the table, 30 s, 45 s and 60 s burn. For all the variants the thrust was equal, 15 kN.

The goal is to assess would yield the best result in terms of altitude. Mission goal for vehicle using this engine is to carry scientific instruments to the mesosphere. Mesosphere extends from 50 km up to 85 km. The target altitude is therefore within these limits.

Approach to determine the peak altitude of the sounding rocket was as follows. Using equation 3.18 the acceleration at any time can be found.

$$F = \frac{m}{a} \tag{3.18}$$

The overall forces acting on the rocket during the propelled flight are the thrust of the engine T, drag force F_D and weight of the rocket W. The acceleration at given time can be therefore found from the following equation (3.19):

$$a_n = \frac{T_n - F_{D,n} - W_n}{m_{tot,n}} \tag{3.19}$$

Subscript n serves as a designation of the increment, starting at $n = 0$ and finishing at the burn time. The engine's thrust T_n is considered constant at the value 15 kN. The acting drag force and weight can be found via 3.20 and 3.21.

$$F_{D,n} = \frac{1}{2} \cdot \rho \cdot v_n{}^2 \cdot C_D \cdot A \tag{3.20}$$

$$W_n = g \cdot m_{tot,n} \tag{3.21}$$

The altitude and the velocity can be found via 3.22 and 3.23.

$$v_n = h_{n-1} + a_{n-1} \cdot \Delta t \tag{3.22}$$

$$h_n = h_{n-1} + v_{n-1} \cdot \Delta t \tag{3.23}$$

Upon reaching the burnout time, the equation 3.18 is no longer viable, as the engine no longer provides thrust and the rocket enters coast phase of the flight. Rocket will continue to coast towards the peak altitude and equation 3.18 must be adjusted. The peak altitude is reached when the rocket velocity is equal to zero, the coast flight phase is finished and rocket begins it's descend.

$$a_n = \frac{-F_{D,n} - W_n}{m_{tot,n}} \tag{3.24}$$

Specific impulse and ideal O/F ration for the paraffin/LOX propellant combination can be found in The weight and mass flow of the oxidizer and oxidizer were determined in the previous section 3.1 and can be found in the table 3.2

Weight of the construction and payload are hard to determine, therefore are estimated at 0.7 times the weight of the propellant for all burn time variants and weight of the complete rocket for the sake of peak altitude analysis was found as follows:

$$m_{rocket} = m_{prop} + 0.7 \cdot m_{prop} \tag{3.25}$$

The peak altitude and the altitude where the engine burned out are listed in the table 3.3.

$t_b(s)$	h_{out} (km)	h_{max} (km)	t_{peak} (s)	m_f (kg)	m_{ox} (kg)	m_{empty} (kg)
30	18.362	82.789	113.8	46.64	116.61	114.28
45	26.244	115.091	134.5	69.96	174.92	171.42
60	32.62	124.188	136.6	93.29	233.22	228.56

Table 3.3: Feasibility analysis results

Results discussion: As we can see from the table 3.3 even the 30 sec-

ond burn version of the rocket would be able to climb almost to the upper stages mesosphere, therefore all of the options could be deemed viable, however the calculation model used is simplified and the real peak altitudes for each option would be somewhat lower in reality. The greatest discrepancy is the the drag force F_D. The cross-section area of the rocket was difficult to determine, during the calculations a constant 5 millimeters were added to the outer radius of the fuel grain for all options. Drag coefficient C_D was considered to be constant throughout the whole flight, which contradicts the real conditions. Numerical and experimental data show that C_D rises with the Mach number of the aircraft.
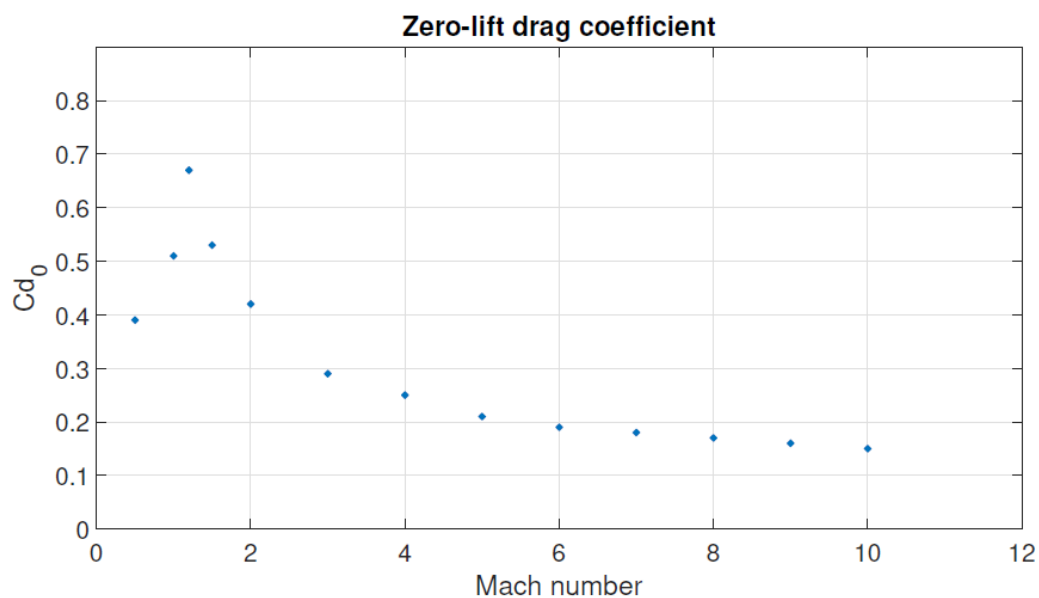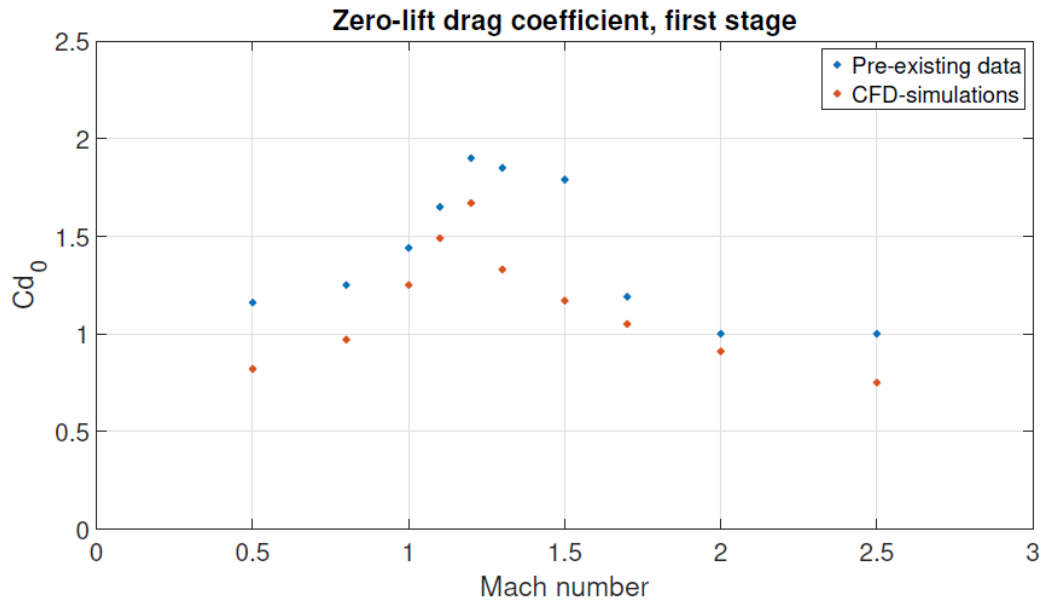

Figure 3.1: Cd_0 for Maxus sounding rocket [5]

Figure 3.2: Cd_0 for Terrier-Black sounding rocket 1st stage [5]
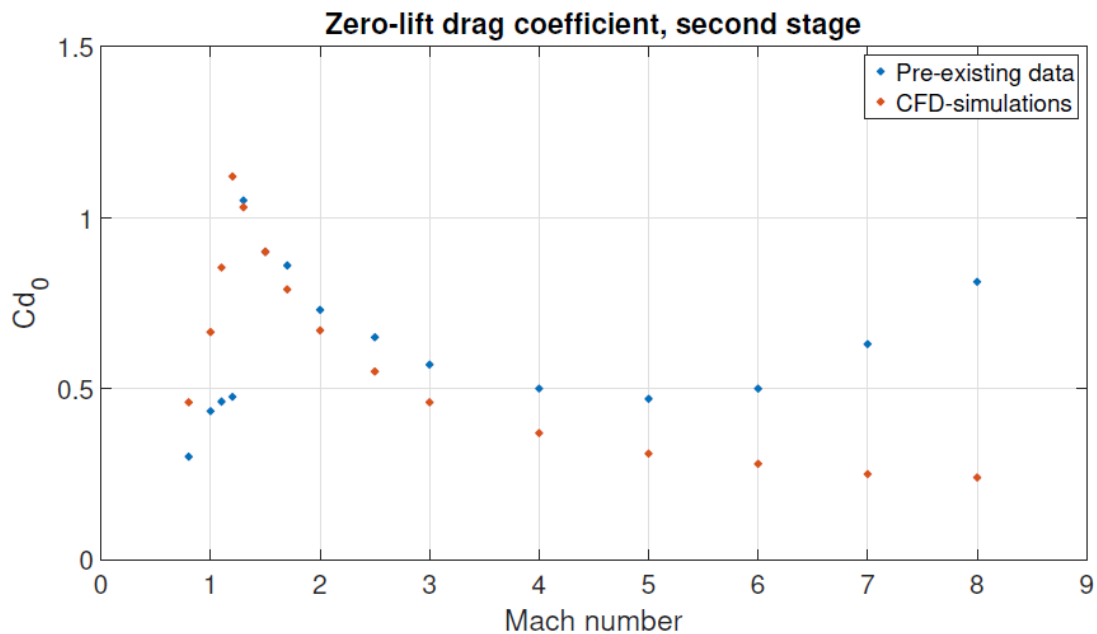
Figure 3.3: Cd_0 for Terrier-Black sounding rocket 2nd stage [5]

As we can see in the figures 3.1, 3.2 and 3.3 based on the CFD simulations of sounding rockets performed in the [5] C_D varies throughout the flight. Based on the data the average C_{D0} varies from 0.32 to 1.1, estimate we have made, C_D=0.5 can be considered viable for use in my calculations, but for more precise results more detailed analysis beyond scope of this thesis would have to be done.

3.3   Nozzle and Combustion Chamber Design

To asses the design of the combustion chamber and nozzle concept of the ideal rocket propulsion was utilized. Thermodynamic principles are expressed using mathematical equations, which theoretically describe the quasi-one dimensional nozzle flow. This is an idealization of the real behaviour of the full three dimensional flow equations. "In designing new rockets, it has become accepted practice to use ideal rocket parameters which can then be modified by appropriate corrections,..."[3]. For idealizing the flow following assumptions are in place [3]:

- Chemical reaction products are homogeneous

- Working fluid is in a gaseous phase, any other phases add negligible amount to the total mass

- Working fluid obeys the perfect gas law

- The flow is adiabatic

- Boundary layer effects and friction are neglected

- There are no shock waves or discontinuities in the nozzle flow

- The propellant flow is steady and constant. The expansion of the working fluid is uniform and steady, without vibration. Transient effects (i.e., start up and shut down) are of very short duration and may be neglected

- Combustion gasses have an axially ditected velocity

- The gas velocity, pressure, temperature, and density are all uniform across any section normal to the nozzle axis.

- Chemical equilibrium is established within the rocket chamber and the gas composition does not change in the nozzle

3.3.1   Nozzle Geometry

In this section of I am to determine the geometry of the nozzle used for our engine. Based on the calculations from the master thesis of my colleague Ľuboš Jiroušek and his solid fuel grain analysis we know the external diameter of the fuel grain. I assume the following equilibrium.

$$d_{ext,g} = d_{i,c} = d_1 = 0.32 \, m \tag{3.26}$$

Since I know the diameter at the nozzle inlet I can determine the nozzle inlet area A_1.

$$A_1 = \pi \frac{d_1^2}{4} \tag{3.27}$$

$$A_1 = \pi \frac{0.32^2}{4} = 0.08 \, m^2 \tag{3.28}$$

Next I have determined the throat area and the throat diameter. From the equation 3.29 we see the range of the area ratios. I have chosen the the ratio according to the 3.30.

$$\frac{A_1}{A_t} = 3 \div 6 \tag{3.29}$$

$$A_t = \frac{A_1}{6} = \frac{0.08}{6} = 0.13 \, m^2 \tag{3.30}$$

$$d_t = \sqrt{\frac{4 \cdot A_t}{\pi}} \tag{3.31}$$

$$d_t = \sqrt{\frac{4 \cdot 0.013}{\pi}} = 0.13 \, m \tag{3.32}$$

To calculate the nozzle exit area and the nozzle exit diameter I used 3.34 and 3.36, based on the area ratio stated in 3.33. I have set the nozzle expansion as

ϵ=15.

$$\epsilon = \frac{A_2}{A_t} = 15 \div 30 \tag{3.33}$$

From the equation 3.33 I have determined then nozzle exit area and the nozzle exit diameter:

$$A_2 = \epsilon \cdot A_t \tag{3.34}$$

$$A_2 = 15 \cdot 0.013 = 0.2 \, m^2 \tag{3.35}$$

$$d_2 = \sqrt{\frac{4 \cdot A_2}{\pi}} \tag{3.36}$$

$$d_2 = \sqrt{\frac{4 \cdot 0.2}{\pi}} = 0.506 \, m \tag{3.37}$$

Next I have calculated the nozzle length, first for the conical shape, following with the two versions of the bell shaped nozzle.

$$L_{cone} = \frac{r_2 - r_t}{tan\theta} \tag{3.38}$$

$$L_{cone} = \frac{0.253 - 0.065}{tan15° = 0.7} \, m \tag{3.39}$$

d_1	A_1	d_t	A_t	d_2	A_2	L_{cone}	$L_{80\%bell}$	$L_{60\%bell}$
0.32	0.08	0.13	0.013	0.506	0.2	0.7	0.56	0.42

Table 3.4: Basic nozzle geometry

In order to determine the actual shape of the curve of the bell nozzle I used the parametric approach based on the Rao's approximation. The parametric expression for the parabolic curve was adapted from [9].

$$x = ay^2 + by + c \tag{3.40}$$

To find the parameters of the equation 3.44 I have adapted the system of the linear equations from the same source:

$$\begin{bmatrix} 2R_N & 1 & 0 \\ 2R_e & 1 & 0 \\ R_N^2 & R_N & 1 \end{bmatrix} \begin{bmatrix} a \\ b \\ c \end{bmatrix} = \begin{bmatrix} \frac{1}{tan\theta_i} \\ \frac{1}{tan\theta_e} \\ x_N \end{bmatrix} \tag{3.41}$$

X_N is the x coordinate of the inflexion point where the radius r_t and start of the parabolic curve meets and can be found using the expression 3.42. The origin of the coordinate system is in the intersection of the axis of symmetry and the throat plane axis.

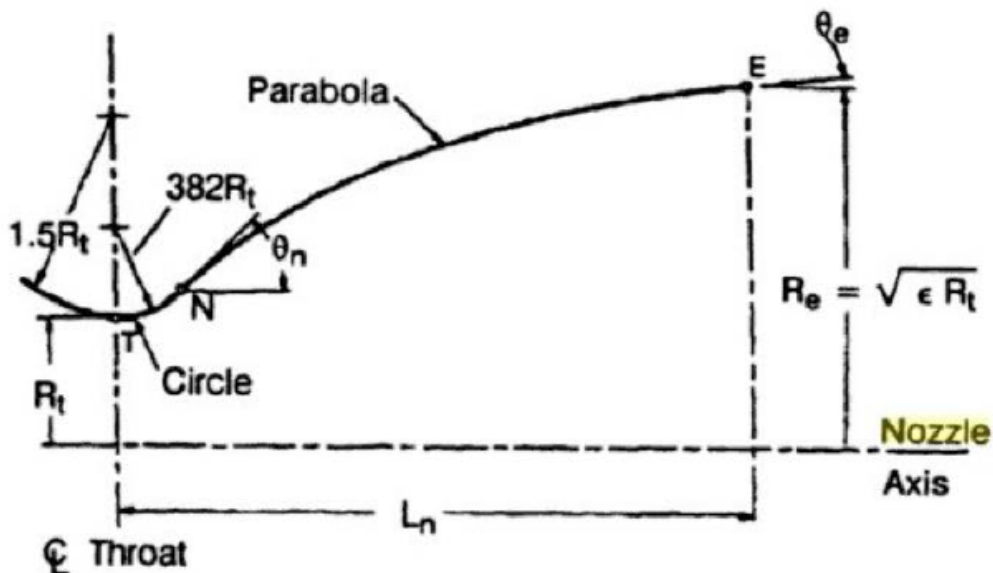$$X_N = 0.382 r_t sin(\theta_i) \tag{3.42}$$

Figure 3.4: Rao's approximation bell nozzle design [9]

By substituting, sample calculation for the 60% bell nozzle, in the equation 3.43 I found the parameters a, b and c.

$$\begin{bmatrix} 2 \cdot 0.0085 & 1 & 0 \\ 2 \cdot 0.2530 & 1 & 0 \\ 0.0085^2 & R_N & 1 \end{bmatrix} \begin{bmatrix} a \\ b \\ c \end{bmatrix} = \begin{bmatrix} \frac{1}{tan32.5°} \\ \frac{1}{tan17°} \\ 1.298 \end{bmatrix} \tag{3.43}$$

Resulting into the following equation of the parabolic curve:

$$x = 3.5814y^2 + 1.516y + 1.2864 \tag{3.44}$$

3.3.2 Nozzle pressure and temperatures

By adjusting the equation 3.45 I can determine the combustion pressure in the combustion chamber and at the nozzle inlet. The adjustment lies in multiplying the characteristic velocity c^*, which can be found in the table 2.1, by correction factor λ based on the nozzle choice resulting in equation 3.46 used to determine the pressure on the nozzle inlet. Correction factor can be found in the 3.5, sample calculation is shown for the conical nozzle in the equation 3.47.

$$c^* = \frac{p_c \cdot A_t}{\dot{m}_{prop}} \tag{3.45}$$

$$p_c = \frac{c^* \cdot \lambda \cdot \dot{m}_{prop}}{A_t} \tag{3.46}$$

$$p_c = \frac{1804.4 \cdot 0.9829 \cdot 5.75}{0.013} = 760\,802\ Pa \tag{3.47}$$

With known combustion chamber pressure I can determine the throat pressure. In the equation 3.48 I have not yet determined the specific heat ratio γ for the combustion gasses. The general chemical composition of paraffin waxes is C_nH_{n+2}. The equation 3.49 describes idealizied combustion process, I assume ideal combustion, therefore only carbon dioxide CO_2 and water H_2O in the form of steam are present on the product side of the equation. Paraffin wax is combusted with oxygen. For this calculation I have assumed $n = 1$.

Area Ratio	10	25	50
Cone (15° Half Angle)			
Length (100%)[a]	8.07	14.93	22.66
Correction factor λ	0.9829	0.9829	0.9829
80% Bell Contour			
Length[a]	6.45	11.94	18.12
Correction factor λ	0.985	0.987	0.988
Approximate half angle at inflection point and exit (degrees)	25/10	30/8	32/7.5
60% Bell Contour			
Length[a]	4.84	9.96	13.59
Correction factor λ	0.961	0.968	0.974
Approximate half angle at inflection point and exit (degrees)	32.5/17	36/14	39/18

[a]The length is given in dimensionless form as a multiple of the throat radius, which is one.

Figure 3.5: Values of the correction factor for several nozzle types [3]

$$p_t = p_c \cdot \left(\frac{2}{\gamma + 1} \right)^{\frac{\gamma}{(\gamma - 1)}} \tag{3.48}$$

$$CH_4 + 4O_2 \Rightarrow 2CO_2 + 4H_2O \tag{3.49}$$
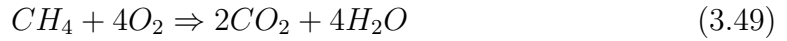
Knowing the combustion products and the ratio in which they are produced during the combustion I can now determine their specific heat at constant volume c_v and specific heat at constant pressure c_p. The relation between specific heats is called specific heat ratio γ and is described by following equation 3.50.

$$\gamma = \frac{c_p}{c_v} \tag{3.50}$$

The values of the c_p and c_v for both steam and carbon dioxide were found in tables, based on the temperature of the gasses. At this point in the design the nozzle temperatures were no yet calculated, I assumed $T_1 = 2500\ K$ and after calculating the temperatures made several iterations to increase the precision of the calculations. After looking up the specific heats for the combustion products I have determined the individual specific heat ratio for each carbon dioxide and steam. To

determine the overall specific heat ratio of the combustion gasses I have calculated the weighted arithmetic mean, based on the amount of the molecules produced during the combustion as seen in 3.51.

$$\gamma_g = \frac{2\gamma_{CO_2} + 4\gamma_{H_2O}}{6} \tag{3.51}$$

Following are the sample calculations for $T = 2800K$:

$$\gamma_{CO_2} = \frac{1.408}{1.219} = 1.155 \tag{3.52}$$

$$\gamma_g = \frac{2 \cdot 1.155 + 4 \cdot 1.09}{6} = 1.112 \tag{3.53}$$

$$p_t = 760\,801.59 \cdot \left(\frac{2}{1.112 + 1}\right)^{\frac{1.112}{(1.112-1)}} = 442\,759\,Pa \tag{3.54}$$

In the design I have assumed the engine to be first used at the atmospheric temperature, hence following assumptions were made:

$$p_2 = p_{atm} \tag{3.55}$$

$$v_2 = c^* \tag{3.56}$$

I have now determined pressure at nozzle inlet, throat and exit. Next I have determined the temperatures at these locations. Temperature at the inlet T_1 I can express from the equation 3.57 and calculated according to the 3.65. The specific molar constant R^* I found via 3.66. To determine the molar mass of the combustion gasses I have, similarly to the approach with specific heat ratio, used the weighted arithmetic mean of the individual molar masses 3.60. From the periodic table: $M_{CO_2} = 44\,g/mol$ $M_{H_2O} = 18\,g/mol$. Alternative approach yielding the same results is to use the c_p and c_v and it's relation to the R^* 3.61.

$$v_2 = \sqrt{\frac{2\gamma}{\gamma - 1} R^* T_1 \left[1 - \left(\frac{p_2}{p_c}\right)^{\frac{\gamma-1}{\gamma}}\right]} \tag{3.57}$$

$$T_1 = \frac{v_2^2 (\gamma - 1)}{2\gamma R^* \left[1 - \left(\frac{p_2}{p_c}\right)^{\frac{\gamma-1}{\gamma}}\right]} \tag{3.58}$$

$$R^* = \frac{R}{M} \tag{3.59}$$

$$M_g = \frac{2M_{CO_2} + 4M_{H_2O}}{6} \tag{3.60}$$

$$R^* = c_p - c_v \tag{3.61}$$

The letter M in the equation 3.60 stands for the molar mass of the combustion gasses, not to be mistaken with Mach number, which is also denoted as M, this is an exception. In the equation 3.60 After I have determined the properties of the combustion gases and the pressures I have calculated the throat temperature T_t using the equation 3.68. In order to find the nozzle exit temperature T_2 I have first calculated the exit mach number M_2 via 3.69. With known M_2 I have found the nozzle exit temperature 3.70.

$$T_t = T_1 \left(\frac{p_t}{p_c}\right)^{\frac{\gamma-1}{\gamma}} \tag{3.62}$$

$$M_2 = \sqrt{\frac{2\left[\left(\frac{p_2}{p_t}\right)^{-\frac{\gamma-1}{\gamma}} - 1\right]}{\gamma - 1}} \tag{3.63}$$

$$T_2 = T_t \left(1 + \frac{\gamma - 1}{2} M_2^2\right)^{-1} \tag{3.64}$$

$$T_1 = \frac{1804^2 \, (1.112 - 1)}{2 \cdot 1.112 \cdot 311.775 \left[1 - \left(\frac{101\,325}{760\,802}\right)^{\frac{\gamma-1}{\gamma}}\right]} = 2\,754 \; K \tag{3.65}$$

$$R^* = \frac{8\,314}{26.67} = 311.775 \; J/kgK \tag{3.66}$$

$$M_g = \frac{2 \cdot 44 + 4 \cdot 18}{6} = 26.67 \; g/mol \tag{3.67}$$

$$T_t = T_1 \left(\frac{442\,759}{760\,801.59}\right)^{\frac{1.113-1}{1.113}} = 2\,616 \; K \tag{3.68}$$

$$M_2 = \sqrt{\frac{2 \left[\left(\frac{101:325}{442\,758.99}\right)^{-\frac{1.116-1}{1.116}} - 1\right]}{1.116 - 1}} = 1.69 \tag{3.69}$$

$$T_2 = 2\,616 \left(1 + \frac{1.116 - 1}{2} 1.69_2^2\right)^{-1} = 2\,244 \; K \tag{3.70}$$

Section	Inlet	Throat	Exit
p [Pa]	760 802	442 759	101 325
T [K]	2 754	2 216	2 244

Table 3.5: Pressure and temperature at different sections of the nozzle, at sea level operation

Now I am able to get more precise approximation of the actual thrust developed by my design, unlike in 3.2 , in which I have estimated the thrust constant throughout the whole flight. Using equation 3.71 I can determine the actual thrust at sea level.

$$T = \dot{m}_{prop} v_2 + (p_2 - p_a) A_2 \tag{3.71}$$

$$T_{h=0} = 5.75 \cdot 1773.54 + (101\,325 - 101\,325) \cdot 0.2 = 10\,198 \; N \tag{3.72}$$

Pressure was determined using the ISA expression, 3.73 for height up to $h = 11\,000\,m$ for after tropopause conditions 3.74 was used.

$$p = p_0 \left(1 - 0.0065 \frac{h}{T_0} \right)^{5.2561} \tag{3.73}$$

$$p = p_{tp} e^{\left(\frac{g h_{tp}}{R^* T_{tp}} \right)} \tag{3.74}$$

The thrust at the sea level can be found in the sample calculation 3.72 and the thrust developed at sea level $T = 10\,198\,N$, the average thrust $T_a = 20\,492\,N$. The course of the thrust over height is plotted in the 3.6.
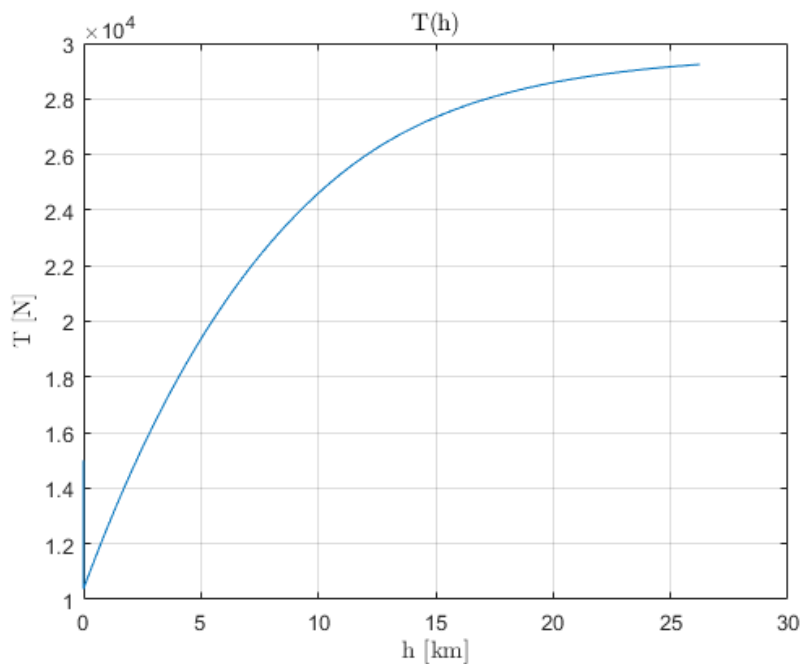

Figure 3.6: Thrust as the function of the altitude until the burnout

3.3.3 Combustion Chamber

The dimensions of the combustion chamber of hybrid rocket engines is largely governed by the solid fuel grain size. Although I have done some analysis of the fuel grain dimensions in order to perform the during the preliminary analysis stage of the design more thorough thought on the grain design was done by Ľuboš Jiroušek, whose Master thesis was concerned with the design and analysis of the fuel

grain and it's combustion. For calculations regarding or referring to the fuel and oxidizer I have adapted his findings. The equation 3.26 states the inner diameter of the combustion chamber. In the subsection 3.3.2 I determined the combustion pressure at the nozzle inlet, I assumed the combustion pressure at the nozzle inlet equal to the combustion chamber pressure. The wall thickness is found using the equation 3.76, apdated from [2].

$$t_w = \frac{(1 + f_s)p_c d_{i,c}}{\sigma} \tag{3.75}$$

As the material for my designed I picked the Inconel 625, nickel-based superalloy. Inconel 625 high strength properties, resistance to elevated temperatures and good protection against corrosion. The ability to retain high yield stress at the high temperatures is crucial for my application, the corrosion resistance is also desirable as the combustion gasses at high temperature usually have higher corrosion and oxidizing effects. This superalloy is used for example in nuclear, marine and aerospace industries. The chemical composition can be seen in figure 3.7. From the data sheet I have decided to place the operating temperature of the engine in the range of $538°C - 760°C$, with a temperature beyond this range the tensile strentgh begins to deteriorate more rapidly. I set the operational temperature at $649°C$. In the data sheet I also found other used values for my calculations, for example the thermal conductivity k for the cooling system design. By substituting in the equation 3.76 I calculated the wall thickness. The factor of safety $f_s = 2$

$$t_w = \frac{(1 + 2) \cdot 0.76 \cdot 320}{413.7} = 1.766 \, mm \tag{3.76}$$

The actual wall thickness was set at $t_w = 2mm$.

Pre and Post combustion chamber

Pre-combustion chamber has an effect on the combustion chamber pressure stability, "chugging" the oxidizer into the chamber without enough space for it to

CHEMICAL ANALYSIS

%	CR	NI	MO	CO	NB+TA	AL	TI	C	FE	MN	SI	P	S
Min.	20	-	8	-	3,15	-	-	-	-	-	-	-	-
Max.	23	Bilance	10	1	4,15	0,4	0,4	0,1	5,0	0,5	0,5	0,015	0,015

Figure 3.7: Chemical composition on Inconel 625 alloy, adapted from Appendix 1

vaporize properly results in oscillations of the combustion pressure, example of this effect can be seen in the picture 3.8. In my design the length of the pre-combustion chamber was designed as a function of the inner chamber diameter $L/D = 0.25$. The combustion chamber is located in the top casing, attached to the combustion chamber and nozzle part via flange and bolts. The L/D ratio is on the lower scale of suitable ratios, the whole issue of the oxidizer injection is in my case closely linked with the ignition system and offers a opportunity for further investigation and study.

Post-combustion chamber serves as a space where yet uncombusted oxidizer and fuel partlices may undergo combustion and also where the combustion gasses mix properly. Similarly to the pre-combustion chamber this part was designed with a link to the length to diameter ratio. Based on the smaller scale experiments I decided to use $L/D = 1$. Post-combustion chamber has a direct effect on the combustion efficiency of the engine, increasing the ratio increases the efficiency. After exceeding the ratio $L/D = 1$ the beneficial effect on the efficiency decreases. The length of the post-combustion chamber was designed to the point where the nozzle convergence starts. With the ratio $L/D = 1$ the expected combustion efficiency is in the range $0.9 \div 0.93$.

3.4 Oxidizer supply

Essentially there are two way of feeding the oxidizer to the combustion chamber. One being the gas-pressurized propellant feed and the other turbopump propellant feed system. In this section both ways will be briefly described and followed by a subsection, in which my conceptual solution will be laid out.

- **Gas pressure feed systems:** In this simple and very common was of pressurizing the oxidizer tank the oxidizer is pushed out of the tank by a pressurant gas, which is fed into the tank at a controlled pressure and thus giving a controlled oxidizer discharge. Simplicity of this feed method comes hand in hand with reliability. The gas pressure feed system usually consists from a high pressure tank, with the pressurant, gas starting valve, followed by a pressure regulator, propellant tank, propellant valves and feed lines. Depending on the mission requirements the complexity of the system might increase and implement additional components, check valves, pressure gauges and so on. For use in gravity-free conditions the propellant tank employs devices to ensure wetting of the propellant outlet. This methods include movable pistons, flexible bladders or surface tension screens.

- **Turbopump feed systems:** As the name suggests propellants are pressurized by pumps, which are powered by turbines deriving the necessary power from the expansion of the hot gasses. This systems is suitable for high thrust applications with long operational duration. The mass of the system is independent of the duration, unlike the gas pressurized tanks, where with prolonged duration mass of the tanks increases. Overall the turbopump solution is more complex, with large amount of components. Based on the management of the combustion gasses there are open or closed loop cycles. In the open loop cycle the working fluids gasses are dumped overboard, in closed loop they are eventually injected into the combustion chamber for increased efficiency.

3.4.1 Oxidizer supply design

First thing I did during the oxidizer supply calculations is to determine the oxidizer pressure, at which it must be fed to the combustion chamber. For this I used equation 3.77 adapted from [2].

$$p_{ox} = 1.2p_c \tag{3.77}$$

The pressure difference $\Delta p \approx 0.2p_c$ represents the total pressure loss in pipes, valves and injection, this expression is amplifying the pressure loss in order to avoid flow instabilities. In my design I have latter on, in the section 3.7 designed the cooling system, where the oxidizer is used as coolant and up-down cooling flow is utilized. This means that coolant enters the piping at the beginning of the combustion chamber, flows "down" through the piping towards the nozzle exit and through an adjacent pipe flows back "up" into the combustion chamber top casing and injector. This design results in a fairly long flow path of the oxidizer, therefore I have decided to increase the presumed pressure difference due to piping and valves. For my calculations I have assumed the pressure difference as $\Delta p \approx 0.75p_c$, the pressure in oxidizer tank can be seen in 3.78. As the shape of oxidizer tank I have initially assumed spherical shape. The inner diameter and wall thickness are determined with following expressions:

$$p_{ox} = 1.75p_c = 1.75 \cdot 760\,801.99 = 1\,331\,403\ Pa \tag{3.78}$$

$$D_{ox,in} = \sqrt[3]{6\frac{V_{ox} + V_u}{\pi}} \tag{3.79}$$

The ullage volume has been assumed as $V_u = 0.05V_{ox}$. This assumption was made based on the information found in [3] and [1], where ullage volume ranges from $2-6\%$, based on the propellant and tank, my assumption is closer to he higher estimate, taking in account potential residual fluid in the tanks.

$$D_{ox,in} = \sqrt[3]{6\frac{0.137 + 0.05 \cdot 0.137}{\pi}} = 0.65m \tag{3.80}$$

$$t_{ox,w} = \frac{0.25\,(1 + f_s)\,p_{ox}D_{ox,in}}{\sigma} \tag{3.81}$$

$$t_{ox,w} = \frac{0.25\,(1 + 1.5)\,1\,331\,403 \cdot 0.65}{225} = 0.0024\,m \tag{3.82}$$

The diameter of the tank is exceeding the outer diameter of the connecting flanges, this is unacceptable, given my constraint the diameter of the tanks should not exceed the flanges outer diameter. Spherical tank is advantageous in certain aspects, but increasing the final diameter of the rocket would bring additional drag force and demean the overall performance of the rocket. To comply with the diameter constraint I decided to use a cylindrical tank, with ellipsoidal head.

$$V_{cyl} = \pi r_{cyl}^2 h_{cyl} + 2 \cdot \frac{2}{3}\pi r_{cyl}^2 h_{head} \tag{3.83}$$

In the equation 3.83 I combined the expression for the volume of the cylinder, the first part, and the volume of the ellipsoidal head. The height of the tank head I have assumed as $h_{head} = 0.05h_{cyl}$. By substituting the height of the tank $h = 1.5m$, and expressing the radius:

$$r_{cyl} = \sqrt{\frac{4V_{cyl}}{3 \cdot (\pi h_{cyl} + \pi h_{head})}} = \sqrt{\frac{4 \cdot 0.1433}{3 \cdot (\pi \cdot 1.5 + \pi \cdot 0.005)}} = 0.17\,m \tag{3.84}$$

Nest step is to calculate the thickness required to withstand the circumferential stress and longitudinal stress. The vessel thickness is the greater of these. Correctional factor for the joint type E was assumed as $E = 0.85$, this corresponds to the welded joint at nozzle. Additional factor of safety $f_s = 1.5$ was taken in account.

$$t_c = \frac{p_{ox}r_{cyl}f_s}{\sigma E - 0.6p_{ox}} \tag{3.85}$$

$$t_c = \frac{1\,331\,402.78 \cdot 0.17 \cdot 1.5}{225 \times 10^6 \cdot 0.85 - 0.6 \cdot 1\,331\,403} = 0.0018\, m \tag{3.86}$$

$$t_l = \frac{p_{ox}r_{cyl}f_s}{2\sigma E + 0.4p_{ox}} \tag{3.87}$$

$$t_l = \frac{1\,331\,403 \cdot 0.17 \cdot 1.5}{2225 \times 10^6 \cdot 0.85 + 1\,331\,403} = 0.0009\, m \tag{3.88}$$

The safety factor of the oxidizer tank I have assumed as $f_s = 1.5$, as the material for both oxidizer and pressurant tanks I have decided to use the aluminium alloy 5083. In the calculations I have assumed the alloys yield strength 225MPa. I was not able to find the exact values for the operational temperature, but this type of alloy is used for the pressure vessels operating at low temperatures from $-200°C$.

tank type	m_{tank} (kg)	t_{tank} (mm)	V_{tank} (m^3)	p_{tank}(Pa)
Sphere	8.67	2.4	0.143	1 331 403
Cylinder	7.61	1.8	0.143	1 331 403

Table 3.6: The oxidizer tank design results

For the design of the pressurant vessel I have first done a preliminary analysis with a goal to get an estimate of the tank pressure and volume. The inner diameter of the tank was restricted not to exceed the outer diameter of the combustion chamber flange. Via the adjusted equation of state for the ideal gas 3.89 I determined the amount of substance n_2 of Helium needed in pressurizing tank to be able to pressurize the oxidizer tank at required pressure and volume.

$$n_1 = \frac{p_{ox}\left(V_{ox} + V_u\right)}{RT} \tag{3.89}$$

$$n_1 = \frac{1\,331\,402.78 \cdot (0.143 + 0.143 \cdot 0.05)}{RT} = 80.88\, mol \tag{3.90}$$

$$n_2 = 2 \cdot n_1 \tag{3.91}$$

$$n_2 = 161.76 \, mol \tag{3.92}$$

Using the equation of state for the n_2 I found the pressure value for the inner diameter of the pressurant tank to comply with restriction. I set diameter of the spherical pressurant tank as $D_{pr,in} = 0.4m$. The oxidizer tank diameter was set smaller, in order to reserve some space around the tank for piping.

$$V_{pr} = \frac{4}{3}\pi r_{pr,in}^3 \tag{3.93}$$

$$V_{pr} = \frac{4}{3}\pi 0.2^3 = 0.0335 \, m^3 \tag{3.94}$$

Using the adjusted law of state for the ideal gas I can now determine the pressure inside of the pressurant tank.

$$p_{pr} = \frac{n_2 T R}{V_{pr}} \tag{3.95}$$

$$p_{pr} = \frac{161.76 \cdot 298.15 \cdot 8.314}{0.0335} = 11\,959\,773 \, Pa \tag{3.96}$$

For thickness calculations I assumed $p_{pr} = 12MPa$.

With the helium tank pressure found I can now determine the tank size and geometry.

$$t_{tank} = \frac{p_{pr} r_{pr,in}}{2\sigma} \tag{3.97}$$

$$t_{tank} = \frac{12 \times 10^6 \cdot 0.2}{2 \cdot 225} = 0.0055 \, m \tag{3.98}$$

$$m_{tank} = \left(\left(\frac{4}{3} \pi r_{pr,out}^3 \right) - V_{He} \right) \rho \qquad (3.99)$$

$$m_{tank} = \left(\left(\frac{4}{3} \pi 0.2055^3 \right) - 0.0335 \right) 2\,650 = 7.53\,kg \qquad (3.100)$$

m_{tank} (kg)	V_{tank} (m^3)	t_{tank} (mm)	p_{tank} (MPa)
7.53	0.0335	5.5	12

Table 3.7: The pressurant tank design results

3.5   Oxidizer injection

The injector for liquid engines is a complex issue, where the flows of two fluids must be matched with problems like angles at which the impinging of the fluid droplets happen. The task is a bit simpler for hybrids, where only one of the propellants is fed through the injector. Yet still there are difficulties to address, for example the length of the pre-combustion chamber, which has to be long enough so the oxidizer has enough time to vaporize. Longer pre-combusiton chambers also lowers the pressure oscillations.
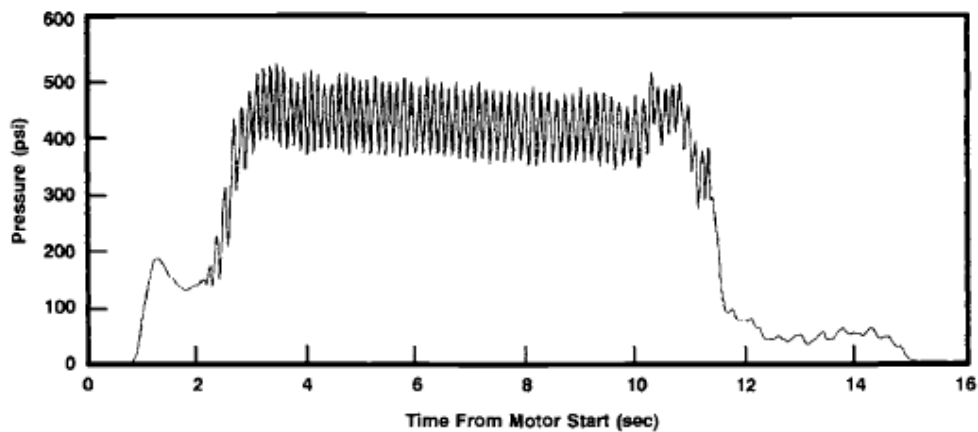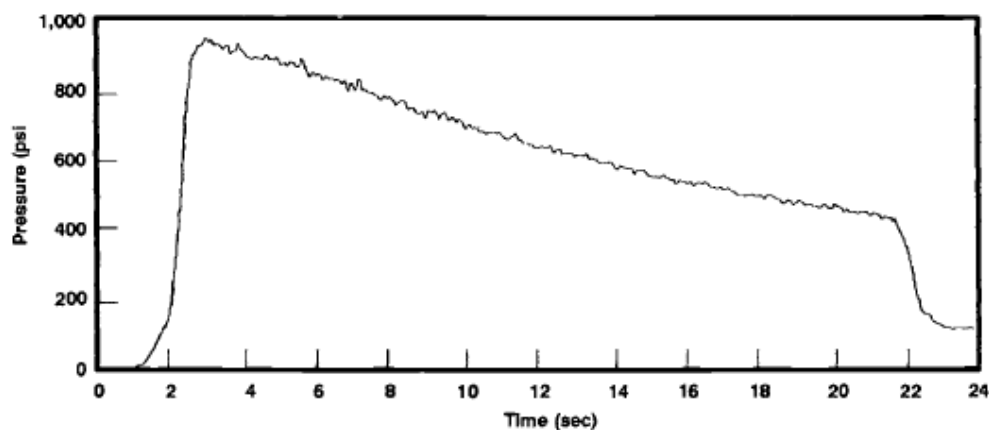
Figure 3.8: Comparison of high and low pressure oscillation operation [3]

Important design factor when it comes to injector design is the discharge coefficient C_d, which describes the ratio between the theoretical and the actual flow through the injector orifice. The discharge coefficient was already determined

38

by experiments for a various number of orifices, its value depending on the orifice shape and the nature of the oxidizer flow. Discharge coefficient values for various orifices can be seen in 3.9.
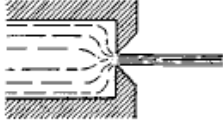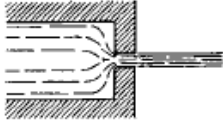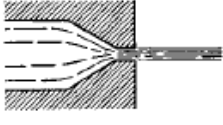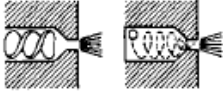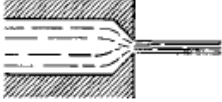
Orifice Type	Diagram	Diameter (mm)	Discharge Coefficient
Sharp-edged orifice		Above 2.5 Below 2.5	0.61 0.65 approx.
Short-tube with rounded entrance $L/D > 3.0$		1.00 1.57 1.00 (with $L/D \sim 1.0$)	0.88 0.90 0.70
Short tube with conical entrance		0.50 1.00 1.57 2.54 3.18	0.7 0.82 0.76 0.84–0.80 0.84–0.78
Short tube with spiral effect		1.0–6.4	0.2–0.55
Sharp-edged cone		1.00 1.57	0.70–0.69 0.72

Figure 3.9: Discharge coefficient table [3]

Based on the values in 3.9 I have decided to use the short-tube with rounded entrance orifice. The corresponding recommended diameter of the orifice $d_o = 1.57mm$, now I can determine the volume flow through one orifice from the equation 3.102. The overall number of the orifices needed to supply sufficient oxidizer flow was calculated from the equation 3.104, adapted from [6] .

$$C_d = \frac{\dot{Q}}{\dot{Q}_{th}} \qquad (3.101)$$

$$\dot{Q}_1 = C_d A \sqrt{\frac{2}{\rho_{ox}} \cdot (p_{ox} - p_c)} \tag{3.102}$$

$$\dot{Q}_1 = 0.9 \cdot \frac{\pi \cdot 0.00157^2}{4} \cdot \sqrt{\frac{2}{1\,280} \cdot (1\,331\,403 - 760\,801.59}} = 3.117 \times 10^{-5}\, m^3/s \tag{3.103}$$

$$N_{or} = \frac{\dot{m}_{ox}}{\rho_{ox} \cdot \dot{Q}_1} \tag{3.104}$$

$$N_{or} = \frac{3.887}{1250 \cdot 3.117 \times 10^{-5}} = 99.77 \tag{3.105}$$

d_o (mm)	Q_1 (m^3/s)	n_{or} (-)	C_d(-)
1.57	3.117×10^{-5}	100	0.9

Table 3.8: Injector design results

3.6 Ignition

The ignition system is crucial for the engine for a number of reasons. Wrong timing of the ignition sequence can for example lead to the hard start with the liquid rocket engines, where during the initial ignition the fuel and oxidizer combination are introduced to the combustion chamber in the wrong ratio and overpressure occurs. This excessive spike in the chamber pressure may lead to structural damage or explosion. Unlike the liquid counterparts the hybrid engines are safer in this regard, as the O/F ratio is governed only by the liquid oxidizer supply and the fuel and oxidizer combinations are typically not hypergolic. The increased safety of the ignition, and safety of storage as there is no need to employ hypergolic substances, is traded-off by different factors complicating the ignition in hybrid rocket engines.

The intial O/F ratio usually varies both in liquids and hybrids from the ideal operational O/F, being somewhat lower at first. There are several viable options, when it comes to ignition systems and the selection process of the suitable specific ignition design depends on many factors. Chiefly being the choice of the fuel/oxidizer combination. The overall design complexity should also be taken in the account, the ignition system should now add unnecessary dry mass or be excessively complicated. It should not burden the vehicle design with additional tanks for additional reactants and piping, in ideal case utilize the substances already on board of the vehicle.

In order for the ignition mechanism to work properly for my choice of propellants it is needed to create a combustible mix of the oxidizer and fuel. Just by introducing the liquid or gaseous oxidizer into the combustion chamber via injector is not enough, as the solid fuel will not mix with the oxidizer and form combustible mix. This is one of the greatest challenges when it comes to hybrid ignition, although it is also one of the greatest advantages of the hybrids, where the low possibility of spontaneous combustion is the very factor increasing the safety of hybrids. It is crucial to ensure the solid fuel to ablate and mix with the flowing oxidizer. This can be achieved by introducing additional energy source. In this section several options when it comes to ignitions systems will be discussed followed by the description of

my conceptual design.

3.6.1 Pyrotechnic ignition

This type of ignition mechanism is probably the simplest, both in design and in operation. Essentially pyrotechnic ignition can be described as a small charge, ignited for example by an electrical current passing through a resistive wire, thus increasing the temperature and igniting the charge. Substances like black powder may be used to create the charge itself. These charges are used for also for example for launching fireworks and smaller version are usually widely available.

Unfortunately the charge can be fired only once, so this type of ignition offers no restartability. Simplicity of the design and operation on the other hand makes this ignition mechanism suitable for smaller scale hybrids, where the even the small charge is sufficient to generate combustible mix of fuel and oxidizer and also ignite the resulting mix. Even though the ignition cannot be repeated once it started it is possible to use for larger scale engines. For example the DARE student club used scaled up pyrotechnic ignition in one of their hybrids. The resistive wire was coated by a substance similar to matches and black powder and covered with steel wool. To prolong the burn of the wool a bypass valve with oxidizer supplies some of the liquid oxygen.

3.6.2 Hypergolic ignition

Hypergolic substances ignite spontaneously upon contact. Hypergolic propellants are well known for their use in liquid engines. As the examples of the combinations can serve unsymmetrical dimethylhydrazine or monomethylhydrazine combined with nitrogen tetroxide. These reactants are probably more famous for their use as propellants rather than ignitors. Used as ignitors they provide reliable source of ignition. However they increase the complexity of the construction by adding additional piping and tanks, also the chance of spontaneous combustion, if the reactants would come in contact sooner and toxicity of the substances lowers

the safety and increase the operation costs. The additional construction might include a precombustion chamber for the hypergols to mix in, shcematics of the engine equipped with the hypergolic ignition can be seen in fig 3.10
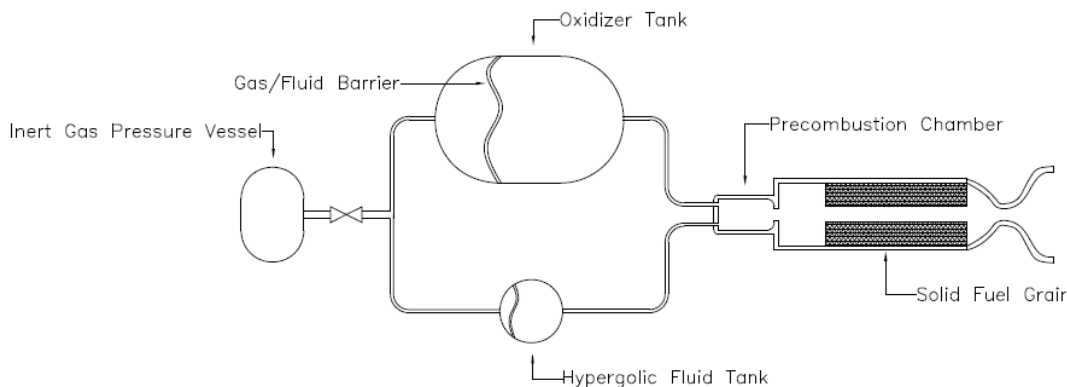

Figure 3.10: Schematics of the hypergolic ignited hybrid engine [4]

3.6.3   Catalytic ignition

During catalytic ignition enough energy is released from the reaction to ensure initiation of the combustion process. With the use of suitable catalyst the specific propellants may be ignited catalytically. Hydrogen peroxide is a typical substance that can be used for this type of ignition. Prior to the combustion chamber a catalytic bed must be located, housing the catalyst in sufficient amount to ensure proper catalytic reaction. Example of a hydrogen peroxide reaction can be seen in 3.106, adapted from [8].

$$2H_2O_2(l) \rightarrow O_2(g) + 2H_2O(g) + heat \qquad (3.106)$$
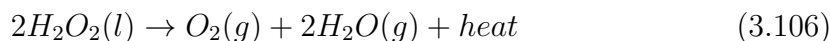
3.6.4   Electrical arc ignition

This type of ignition mechanism utilizes the effect called electrical breakdown, where the insulating medium between high voltage electrodes has been exposed to a voltage higher than its electrical breakdown voltage and an electrical arc is formed between the electrodes. The electrodes can be placed inside of the fuel

grain. After the formation of the arc plasma comes in contact with the fuel grain
surface and the heat of the plasma causes ablation of the solid fuel grain. Now
gaseous fuel products mix with the oxidizer and form combustible mix, once there is
enough of the gaseous fuel present. Plasma also serves as a spark that initiates the
ignition of the fuel and oxidizer mixture. This approach to the hybrid ignition issue
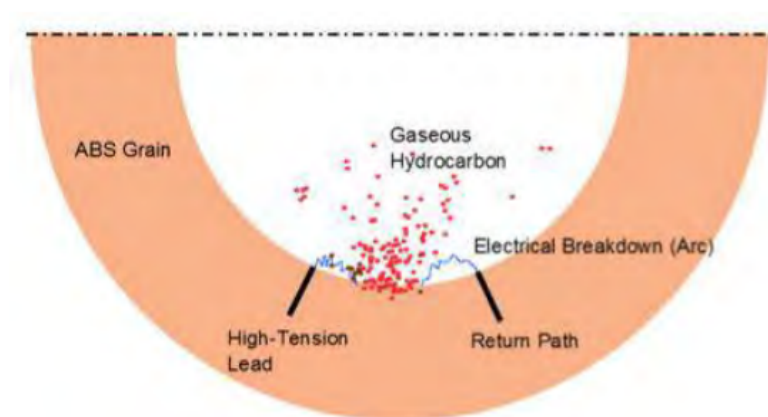utilizes substances already present in the engine and does not require additional
reactants.

Figure 3.11: Visualization of the electric arc ignition on the cross-section of the fuel
grain [7]

3.6.5 Plasma torch ignition

Plasma torches utilize electrical energy to directly heat a flow of a gas
medium and form a high temperature plasma flow. This heated plasma can be
used to ablated the solid fuel grain to produce gaseous fuel particles to be combined
with the oxidizer and form a combustible mixture. Heat of the plasma flow also
serves as initiator of the ignition once the combustible mix is formed, similarly in
principle to the electrical arc ignition. Inside the plasma torch body there are two
electrodes, electrical arc forms between the cathode and anode and working gas
flows through the arc and creates a plasma jet. Simplified schematics can be seen
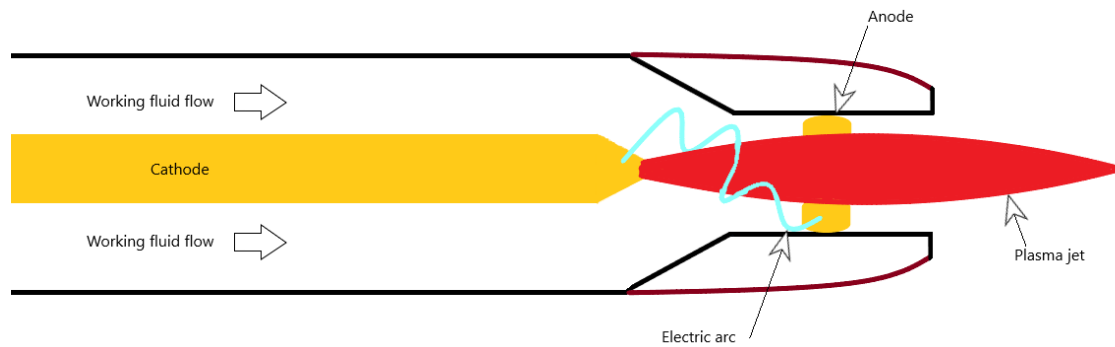in the figure 3.12

Figure 3.12: Plasma torch schematics

3.6.6   Ignition design

For my design I have chosen the plasma torch ignition, this type of igniter was already tested with smaller hybrid engines [12]. Experiments done in this paper found, that plasma jet created by the plasma torch may not be of sufficient length. If the distance between the solid fuel grain and the plasma jet is too long, the heat of the plasma will not be able to ablate the fuel grain. To enlarge the fuel jet the plasma torch nozzle end was equipped with a small ignition-assistant fuel cartridge. This adjustment made the plasma jet large enough to ensure the creation of the combustible and ignition. For my design I have adapted similar solution. Since I have designed the engine with the liquid oxygen as the oxidizer I need the pre-combustion chamber in order to provide space in which the liquid oxygen can evaporate, too small pre-combustion chamber following the injector would lower the efficiency of the combustion. To form a plasma jet big enough I have scaled up the ignition-assistant cartridge. It is difficult to determine the actual ideal length of the resulting flame plume and it would require some testing to tune the actual design. In the oxygen rich environment of the combustion chamber the flame jet formed by ignitor would be enough to ablate at least some of the fuel and initiate first smaller combustion, which would lead to the further ablation and actual engine ignition. As the working fluid of the plasma torch I choose to use Helium, used also as a pressurant gas for pressuring the oxidizer tank.

3.7 Cooling

Because of the high operating temperature and relatively long burn time I have to employ one of the cooling methods to prevent failure. In this section I present a short description of the cooling methods used and in 3.7.1 I present my design for the regenerative cooling for my rocket engine.

- **Regenerative cooling** Probably the most widely applied method of cooling. The propellant or oxidizer, sometimes both, are fed through passages in the thrust chamber and nozzle wall before being injected into the combustion chamber. In my case the only option to use as a coolant is the oxidizer. The fuel grain in hybrids serves as a sort of insulation for the combustion chamber, but the post-combustion chamber and nozzle are exposed to the heat without any additional relief.

- **Dump cooling** In principle similar to the regenerative cooling, but as the name suggests the coolant is dumped overboard. This means only a portion of the propellants can be used for and it also limits the type of propellants to be used in the engine. Typical is the use of hydrogen in LO_2/LH_2 engine.

- **Film cooling** Part of the propellant is introduced directly through the chamber wall via manifolded orifices, forming a thin protective film. This method is employed for engines with high heat fluxes, sometimes in combination with the regenerative cooling. This method would also be viable in my design, since the additive technology would allow interesting possibilities in terms of the orifice and manifold design, however the proper investigation of this possibilities were beyond the scope of this thesis.

- **Ablative cooling** During the ablative process the combustion chamber wall melts, vaporizes and undergoes a chemical change in order to dissipate the heat. By sacrificing the material cooler gases flow over the wall surface, lowering the boundary layer temperature. This method is usually used in the solid engines.

- **Radiation cooling** With this method the heat is simply radiated by the outer surface of the thrust chamber. Usually applied for the nozzle extensions, where the pressure induced stress is lower.
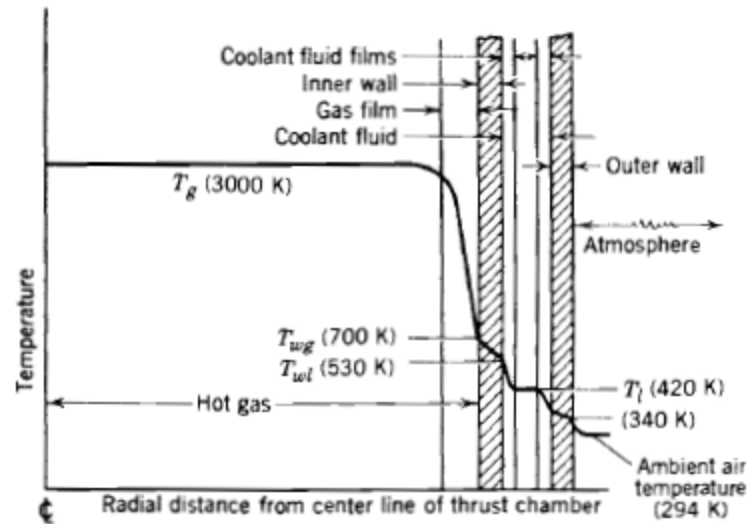

Figure 3.13: Section of the cooled rocket thrust chamber with typical temperatures [3]

3.7.1 Regenerative cooling design

As the cooling method I decided to employ the regenerative cooling, with the oxidizer as the coolant. Because I assume metal additive technology as the fabrication method for my engine, the cooling channels can be implemented in the nozzle and combustion chamber itself. I must calculate the number and area of the coolant passages. To determine this I used the equations found in [3].

$$q = h(T_g - T_l) \tag{3.107}$$

$$q = h_g(T_c - T_{wg}) \tag{3.108}$$

$$q = \frac{k}{t_w}(T_{wg} - T_{wl}) \tag{3.109}$$

47

$$q = h_l(T_{wl} - T_l) \tag{3.110}$$

These equations are generally applicable for the steady-state heat transfer analysis. The gas film h_g and coolant film h_l coefficients can be determined via 3.111 and 3.112:

$$h_g = 0.026 \frac{(\rho v)^{0.8}}{D^{0.2}} Pr^{0.4} \frac{\gamma}{\mu^{0.8}} \tag{3.111}$$

$$h_l = 0.023 \bar{C} \frac{\dot{m}}{A} \left(\frac{Dv\rho}{\mu} \right)^{-0.2} \left(\frac{\mu \bar{C}}{k} \right)^{-\frac{2}{3}} \tag{3.112}$$

Constants 0.026 in 3.111 and 0.023 3.112 are empirically determined.

my approach was as follows. By substituting the t_w from 3.109 I can determine the heat transferred per unit area per unit time. Wall temperature on the gas side T_{wg} is determined by the material constraint of the Inconel 625, according to the data sheet, supplied as an appendix, the major changes in the yield stress due to the temperature occurs between $538°C$ and $760°C$. For my calculations I set acceptable working temperature as $649°C = 922K$. For this temperature and corresponding yield stress I determined the wall thickness t_w, see section 3.3. The conductivity of Inconel 625 at the working temperature foung in the data sheet is $k = 16.4W/mK$.

$$q = \frac{k}{t_w}(T_{wg} - T_{wl}) \tag{3.113}$$

The wall temperature on the coolant side T_{wl} is determined by the boiling point of the coolant, for liquid oxygen $90K$. Upon exceeding the coolant boiling point by $10 - 50K$ phenomenon known as nucleatic boiling occurs. The vapour bubbles form on the wall surface and break away from the wall and collapse in the cooler liquid further from the wall. This causes turbulence in the flow, spoiling the cooling capacity. "The turbulence induced by the bubbles changes the character of

the liquid film and, augmented by the vaporization of some of the propellant, the heat transfer rate is increased without a proportional increase in the temperature drop across the film, ..." [3]. I assumed acceptable liquid side wall temperature as $T_{wl} = 95 K$.
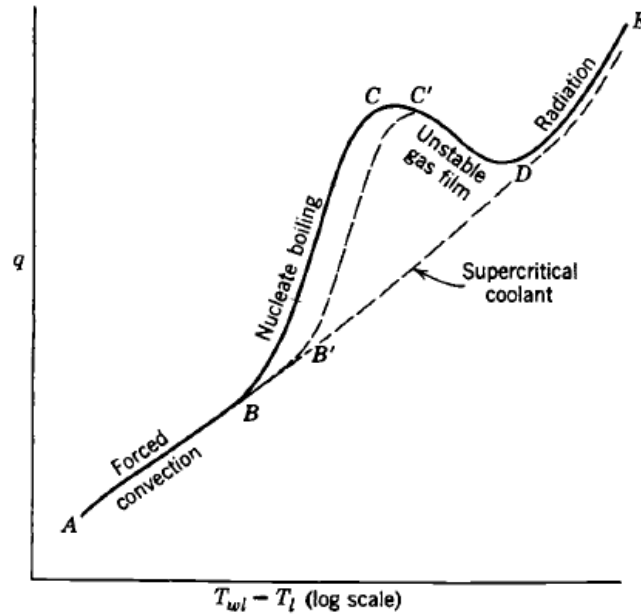

Figure 3.14: Effect of the nucleate boiling on heat transfer [3]

$$q = \frac{16.4}{0.002}(922 - 95) = 6\,789\,600\ W/m^2 s \tag{3.114}$$

By substituting in the equation 3.115 I can determine the h_l.

$$h_l = \frac{q}{(T_{wl} - T_l)} = \frac{6\,789\,600}{(95 - 61)} = 199\,694\ W/m^2 sK \tag{3.115}$$

Now I can determine the required flow area of the coolant passages. By substituting the flow area A from equation 3.112. But first I substituted the flow velocity v and equivalent diameter D as functions of the flow area.

$$D = \sqrt{\frac{4A}{\pi}} \tag{3.116}$$

$$v = \frac{\dot{m}}{\rho A} = \frac{3.75}{\rho A} \tag{3.117}$$

$$A = \left[0.023 C_p \frac{\dot{m}}{h_l} \left(\frac{\dot{m}\sqrt{\frac{4}{\pi}}}{\mu} \right)^{-0.2} \left(\frac{C_p}{k_{LOX}} \right) \right]^{3/4} \tag{3.118}$$

$$A = \left[0.023 \cdot 1670.19 \cdot \frac{3.75}{199\,694} \cdot \left(\frac{3.75\sqrt{\frac{4}{\pi}}}{0.000621} \right)^{-0.2} \cdot \left(\frac{1670.19}{0.194} \right) \right]^{3/4} = 0.0005\,m^2 \tag{3.119}$$

To determine the number of coolant passages I have assumed square shaped passage with dimensions 2.5x2.5 mm at the nozzle throat. With these dimension there is still room for sufficient wall thickness between the adjacent passages. The number of passages is calculated by dividing the area of one passage by the required passage area.

$$A_{pas} = a \cdot a = (2.5 \cdot 2.5) \times 10^-6 = 6.25 \times 10^-6 m^2 \tag{3.120}$$

$$N = \frac{A}{A_{pas}} = \frac{5 \times 10^-4}{6.25 \times 10^-6} = 81 \tag{3.121}$$

Coolant passages were designed to widen with increasing diameter, turning from the square shape at the throat into ring segment at nozzle exit. The combustion chamber and nozzle are designed as one piece, same ideological approach in terms of the cooling applies therefore to the combustion chamber. The oxidizer inlet into cooling passages is through a tube connected to a flange at the nozzle exit. In the flange there is a rectangle shaped duct serving as a coolant manifold. The manifold duct travels along the entire nozzle exit diameter to distribute the coolant into individual passages. The wall thickness at the manifold duct is increased in order to mitigate the potential threat of mechanical damage during manipulation. Coolant travels through passages against the combustion gasses flow direction up the nozzle and combustion chamber. In the connecting flange, where the combustion chamber connects with the casing, is another rectangle manifold duct. From the manifold

duct there are 24 orifices, which ensure the oxidizer flow into the casing and into the injector located in the casing. The connection between combustion chamber flange and casing flange is sealed using the PTFE sealing rings, this material is used as sealant in cryogenic applications with liquid oxygen and is able to withstand the cryogenic temperatures. Both manifold ducts and internal pipes in the casing have approximately same cross section area as the required coolant flow area.

The presented design is of the cooling system is sufficient for a conceptual design phase, but it would be desirable to further investigate, fro example better optimization in term of coolant flow analysis, losses due to the flow and friction in the passages would be in place and offers opportunity for further study. Also further analysis of the combined regenerative and film cooling might be in place.

3.8 Design summmary

In this section figures of the final design are presented with complementary description of the engine's subsystems. First two figures 3.15 and 3.16 are the whole engine assembly, in the second case put in a representative fuselage, shown as a section with a person to scale.

Following the assembly are the figures of the subsystems itself in a order as were described in the thesis, starting with the combustion chamber and nozzle. The nozzle flange has 24 holes for bolts. Half of these is to be used to connect the combustion chamber to the head casing, the other half is meant as a connecting points for the fuselage. The combustion chamber and nozzle is meant to be fabricated using the metal additive manufacturing. With the overall combined length of the nozzle and combustion chamber over 2 meters, using metal additive manufacturing the actual possibility of printing the combustion chamber and nozzle as one piece seems distant. Metal 3D printers usually operate with volumes of several hundred millimeters, the largest up to 1 000x1 000x700mm. Taking into account possible developments in the field, in several years the manufacturing might be possible. To adjust these technological limitations the nozzle could be split from the combustion chamber and reattached using flanges, similar to the one used for the connection of the combustion chamber and head casing. To split the length evenly, the section would take place probably at the beginning of the pre-combustion chamber. The fabrication speeds of the metal 3D printers varies greatly, between $100 cm^3/hour$ up to $12\,000 cm^3/hour$ for the fastest machines. To consider the possible print time, let's assume the part as a cylinder, with the diameter equal to the outer diameter of the nozzle exit flange and length of 2 meters.

$$V_{print} = LD^2\pi 0.25 = 2 \cdot 0.6^2 \cdot \pi \cdot 0.25 \approx 0.6 m^3 \tag{3.122}$$

$$t_{print} = \frac{V_{print}}{v_{print}} = \frac{600\,000}{100 \div 12\,000} = 6\,000 \div 50 hr \tag{3.123}$$
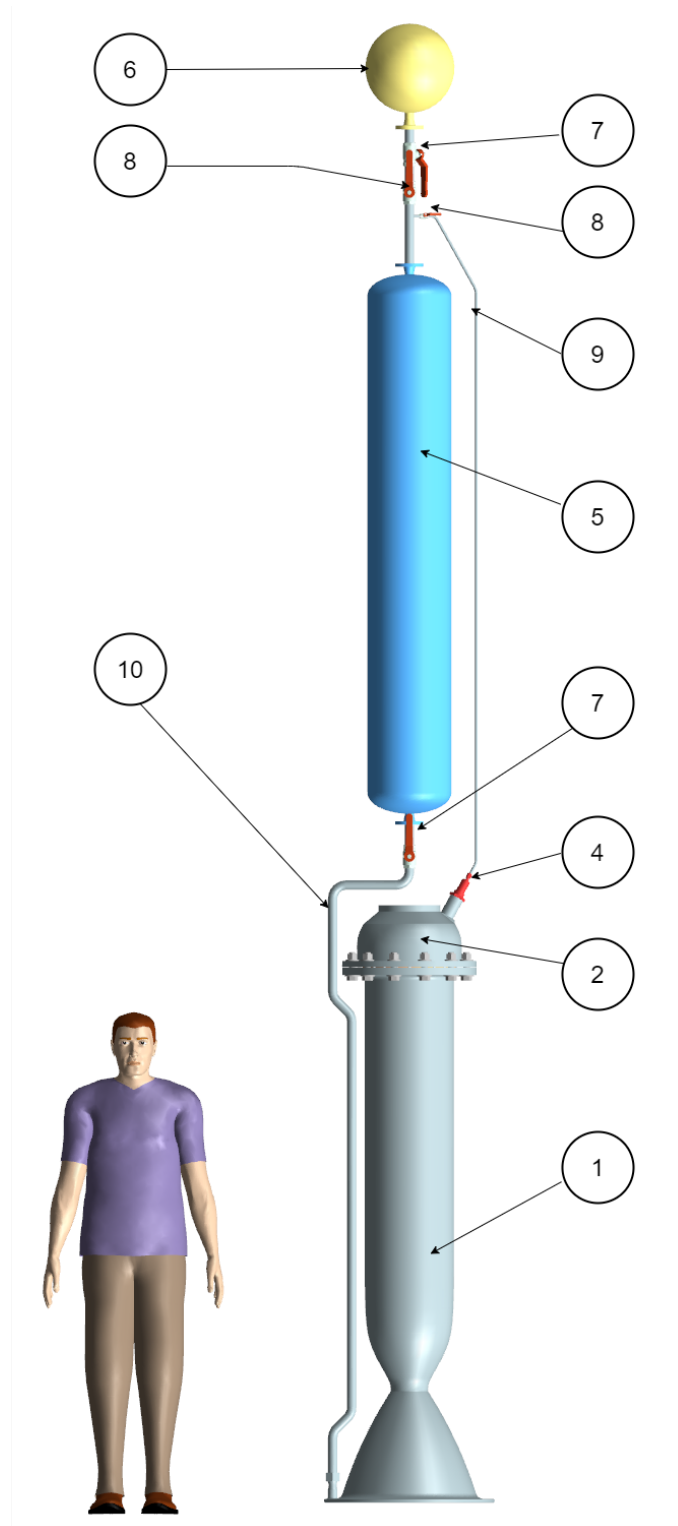
Figure 3.15: Engine in assembly: 1 - Combustion chamber and nozzle, 2 - Head casing, 4 - Igniter, 5 - Oxidizer tank, 6 - Pressurant tank, 7 - Shut-off valve, 8 - Pressure regulator, 9 - Helium bypass duct, feeding the igniter, 10 - Oxidizer duct, person to scale
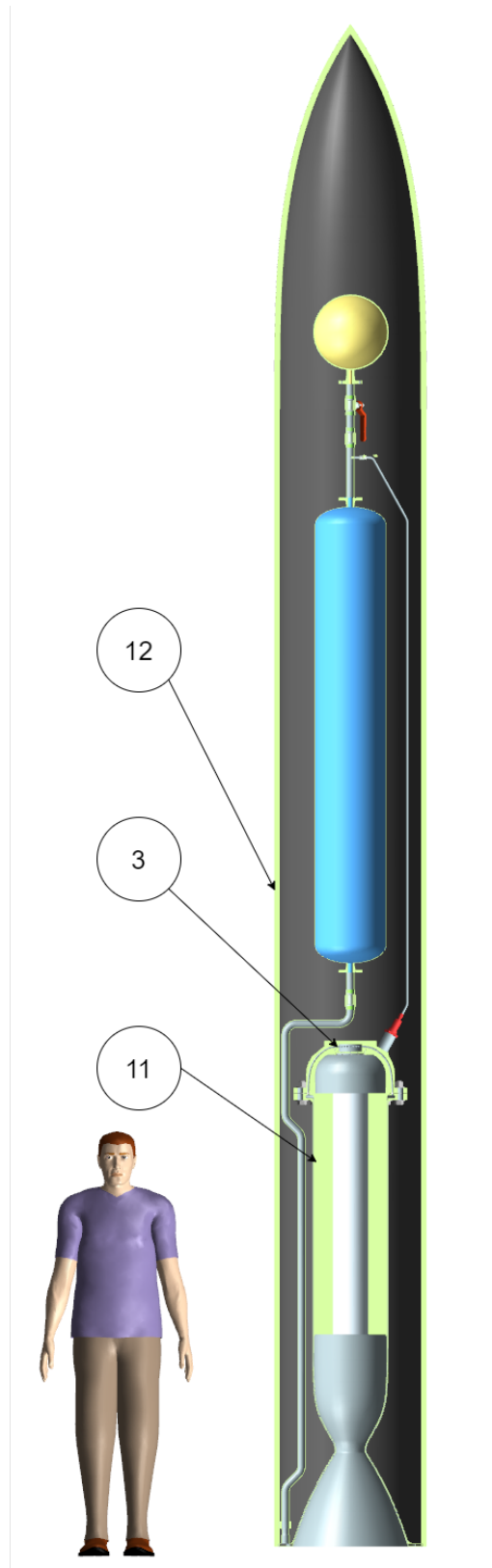
Figure 3.16: Assembled engine in a representative fuselage, 3 - Injector, 11 - Fuel grain, 12 - Fuselage
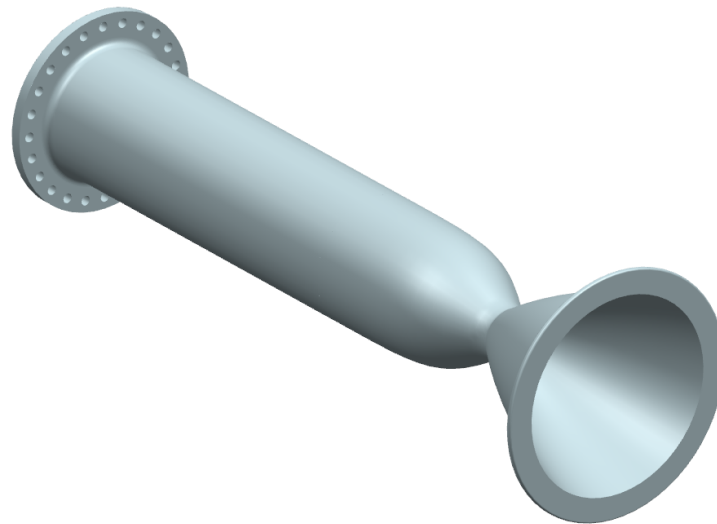
Figure 3.17: Combustion chamber and nozzle

The printing of the nozzle as is would therefore be take up probably some-time between 6 000 and 50 hours. The operation might be faster considering the thin walled design of the nozzle. The detailed section of the oxidizer inlet into the cooling passages can be seen in the 3.19. In the middle of the ducted flange we can see the thickening rib, several ring section shaped ribs are inside the ducted flange, to help withstand the mechanical loads.
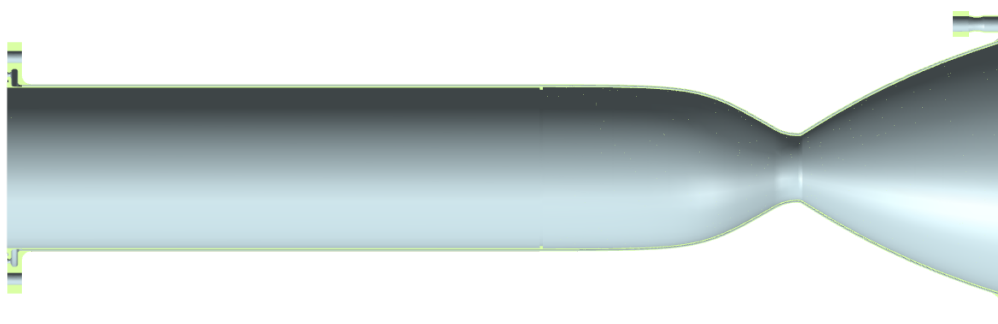
Figure 3.18: Section of of the combustion chamber nozzle, flange on the left hand side to be connected with head casing, right hand side is the ducted flange with oxidizer inlet

From the roughly rectangle shapes of the passageways at the nozzle exit plane the shape changes into roughly square at the nozzle throat plane, 3.20.

The transfer of the oxidizer between combustion chamber and the head
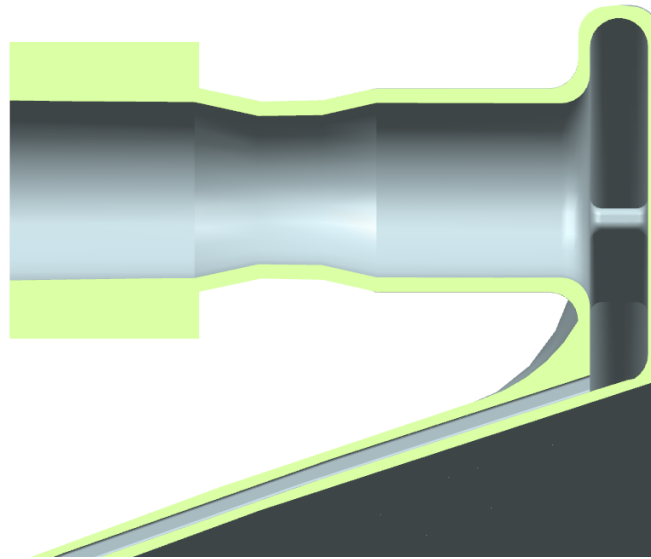
Figure 3.19: Detailed view of the nozzle oxidizer inlet
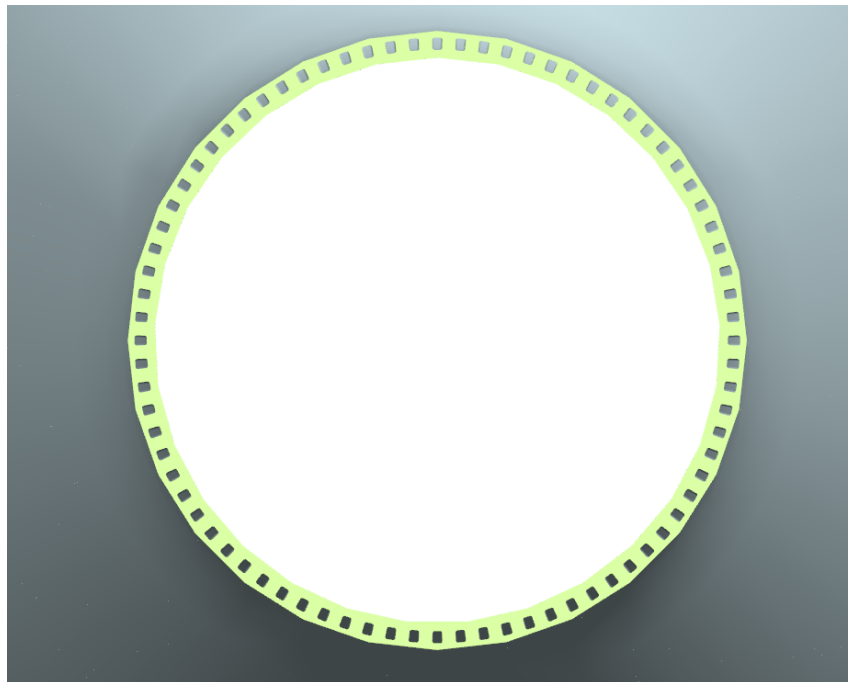
Figure 3.20: Throat plane section of the nozzle

casing, where it flows into the injector, is done via the connecting flange. In a similar fashion of the ducted flange at the nozzle exit there is rectangle shaped duct inside the flange. There are 22 orifices connected to the radial duct. These orifices are linked to the ducts inside head casing, leading the oxidizer to the injector plate. Each orifice is sealed using PTFE sealing rings, fitting into the slot around orifices. The flanges itself have slot for a copper seal, in the figure seen below the oxidizer

flow path.
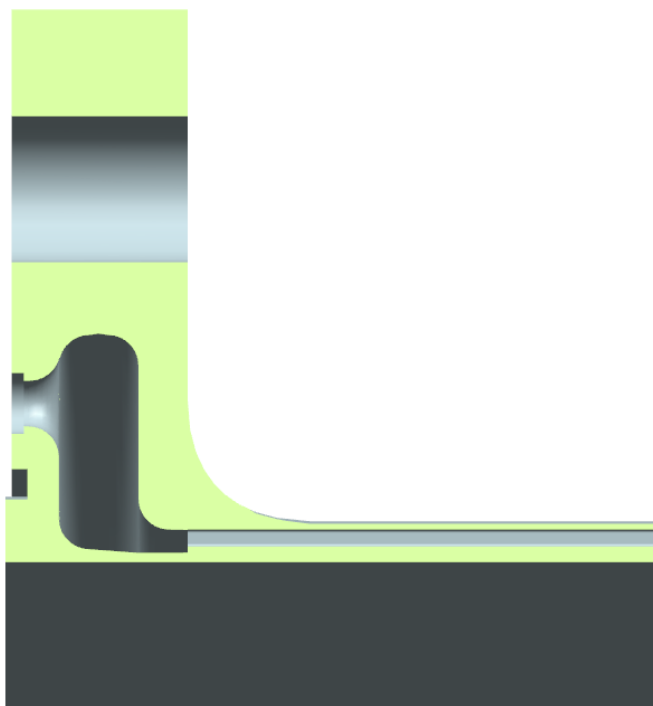
Figure 3.21: The detailed section of the connecting flange

The engine equipped with headcasing and loaded with fuel grain can be seen in the figure 3.22. The fuel grain is to be loaded from the head casing side, at the end of the combustion chamber there is ledge for the grain to lay upon. From the side the grain is secured with the head casing. Pre-combustion chamber is relatively small, the oxidizer injection and dispersion of the gaseous oxidizer could be optimized, but this would require flow analysis and experimental verification. Based on the data from the tests and flow analysis the pre-combustion chamber might undergo optimizing.

The injection plate has 100 radially arranged orifices, one in the middle and rest on the concentric circles, 10 on the first, 20 on the second, 30 on third and 39 on the last. The injection plate is mounted into the head casing by using 12 bolts, threaded holes are in the head casing. The injection plate is equipped with two slots for the sealing, one on the head casing side, the other on the cylindrical plate.

The representative model of the ignition torch can be seen in 3.26, mounted in the head casing. During the experiments conducted by [7] the torch itself was not
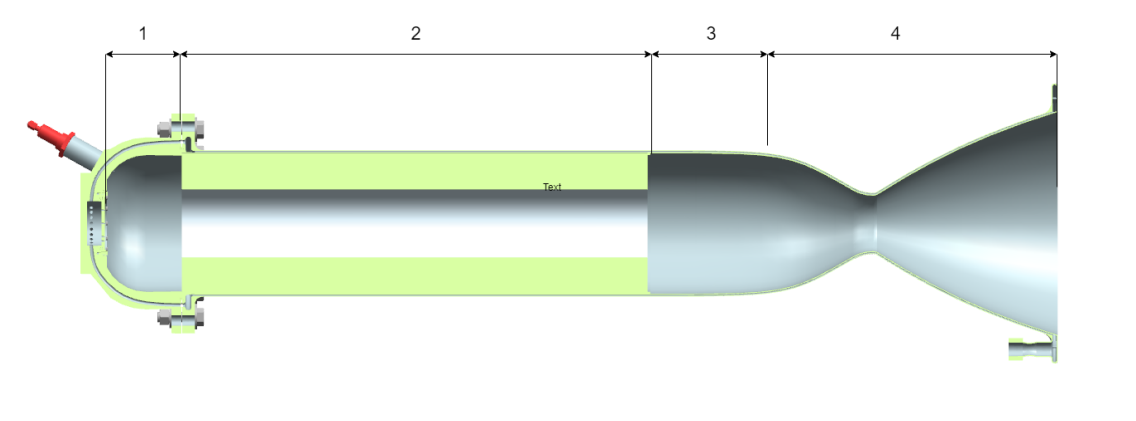
Figure 3.22: Section of the engine, with head casing attached and fuel grain loaded, 1 - Pre-combustion chamber, 2 - Combustion chamber, 3 - Post-combustion chamber, 4 - Nozzle

able to light the tested engine, small piece of plastic was added to the nozzle end of the torch to increase the flame length a introduce enough heat to he fuel surface. In my design I have taken similar approach. The tested plasma torch was fed by argon gas, in my case it would be fed by helium, used as pressurant, fed into the plasma torch from a bypass, duct travelling along the oxidizer tank, visible in the 3.15. According to the [7] helium should be able to perform as working gas same way as argon did during the experiment. The additional issue this solution brings is the additional weight, because the plasma torch requires significant power supply. On the other hand this solution brings the advantage of the longer burn of the torch. During the experiment the torch was able to burn for 5 seconds, even with small ignition assistant. The fuel pellet in my design was scaled up a bit. The torch itself is mounted into head casing via the threaded hole. This system would also require further investigation a optimization, without experiments it is hard to determine the actual length of the flame and it's effect on the solid fuel grain. This goes hand in hand with the head casing design and the pre-combustion chamber design. If the flame developed by the flame would be of large extent, the pre-combusiton chamber could be bigger, allowing better vaporization of the liquid oxidizer, if the oxidizer would still require more space, the igniter could be moved closer to the flange and fuel grain. Possibility to increase the ignition assistant in size is limited by the fact that through the head casing leads the oxidizer flow. Too great increase in the fuel
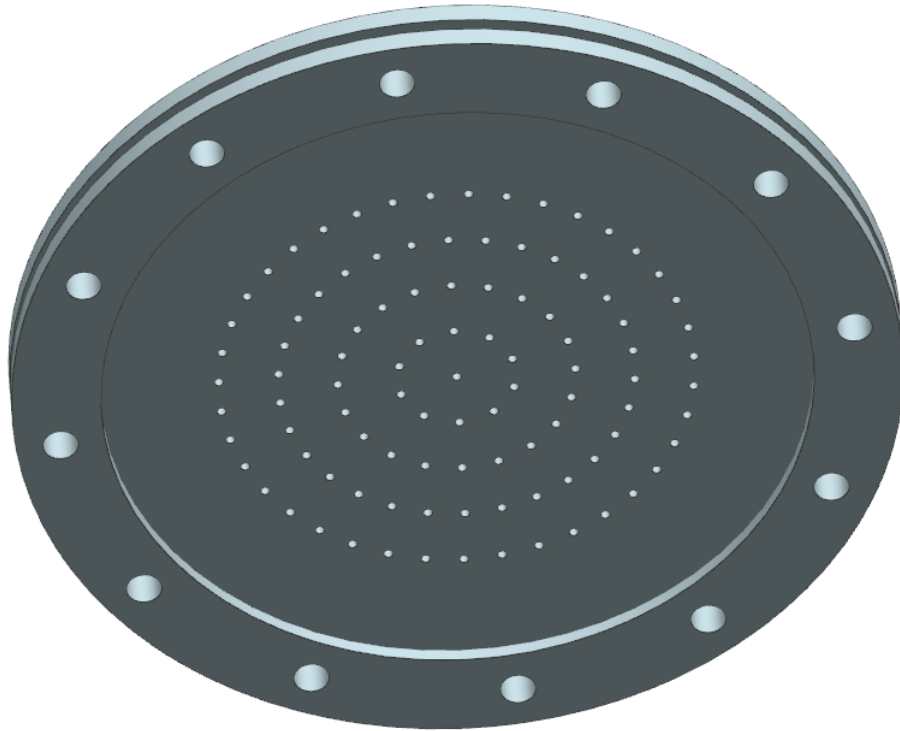
Figure 3.23: The oxidizer injection plate- "shower head" type, shown from the combustion chamber side
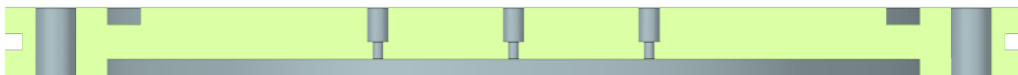

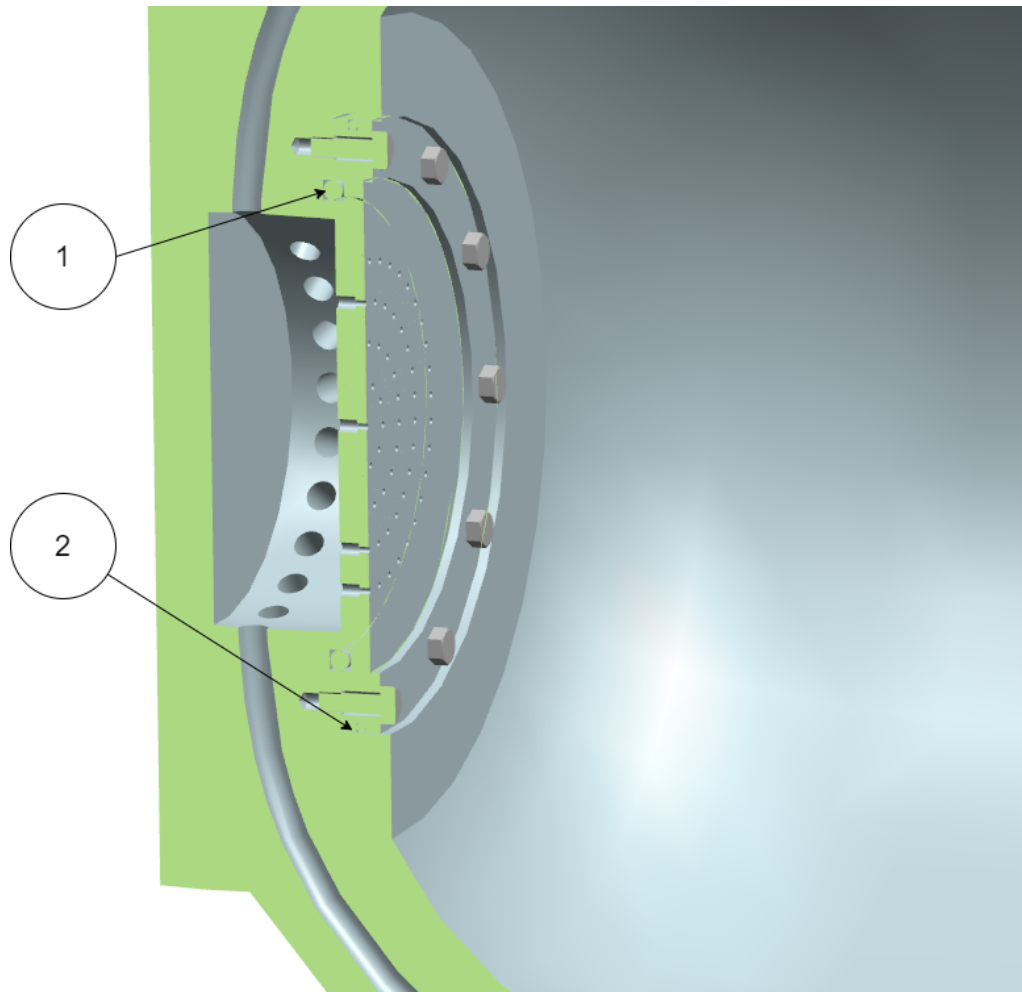Figure 3.24: Section of the injector plate

Figure 3.25: Section of the mounted injection plate in the head casing, 1 - primary seal, 2 - secondary seal
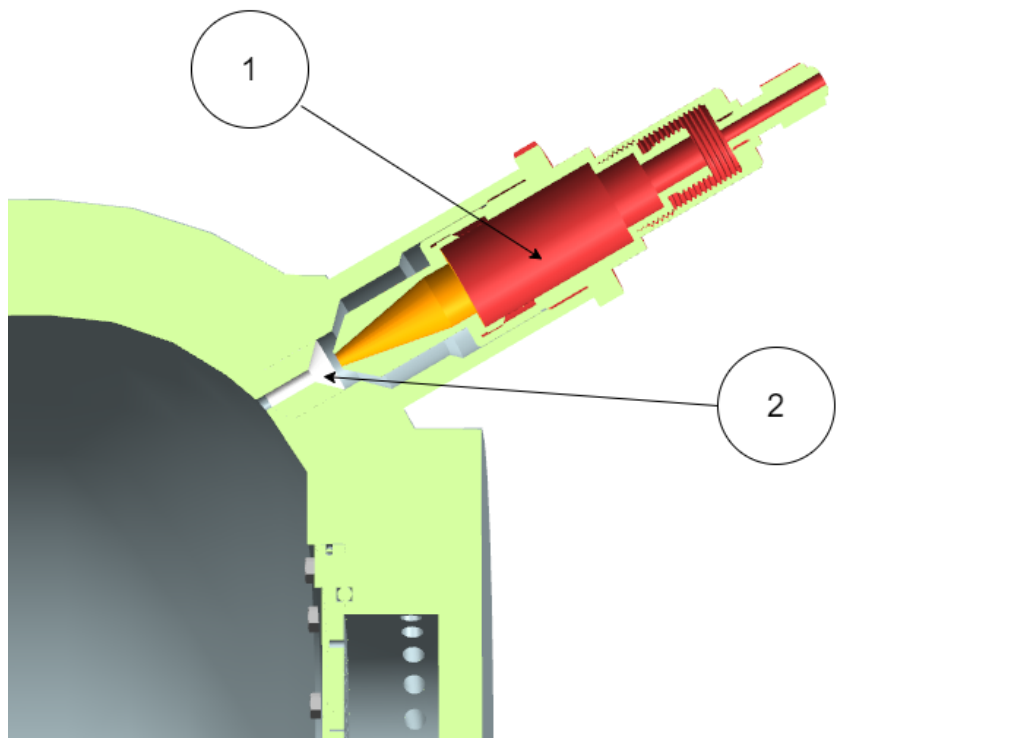
Figure 3.26: Section of the igniter, 1 - Plasma torch, 2 - Fuel pellet

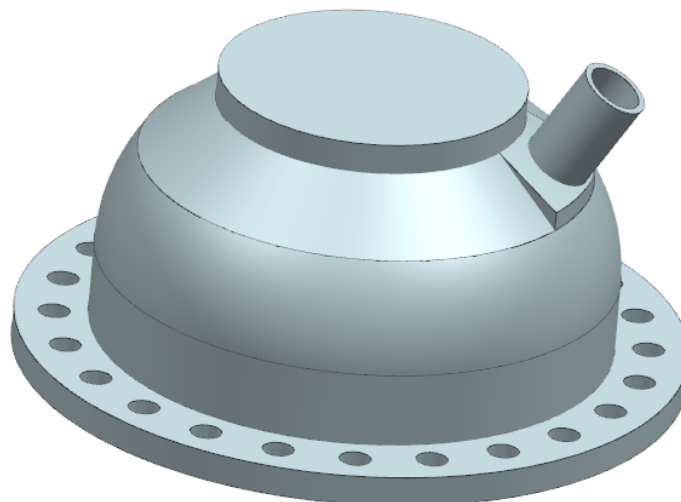pellet size would result in reducing the duct flow area.

Figure 3.27: Chamber head casing

In my design the engine head casing is also to be 3D printed. This offers a opportunity to save weight, while the bulky solid body as can be seen in the 3.27 would weigh around 90 kilograms, 3D printed structure would offer great weight savings, beside the connecting flange it is not necessary to use so much material, in a similar fashion in which the oxidizer ducts are made, the weight saving channels could be manufactured. The flange still needs to retain most of the mass, but other than that head casing can be turned into thinner structure, with a wall thickness similar to combustion chamber and nozzle. Using different fabrication methods would render the fabrication of the oxidizer passages in the head casing near impossible.

In the figure 3.29 the detailed section of the flange connection is depicted, with the connection between head casing passages and combustion chambers channel visible. Typical way of connecting head sizing to a combustion chamber is depicted in the figure 3.28, only half of the holes are being used at the moment, the rest is to be used to mount and attach the engine into the rocket or to the test stand.
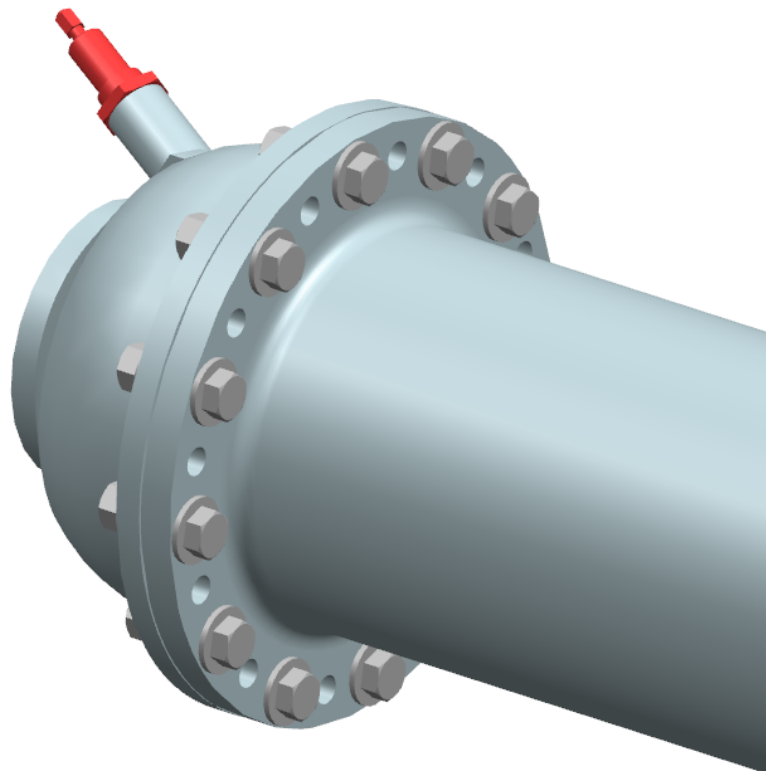

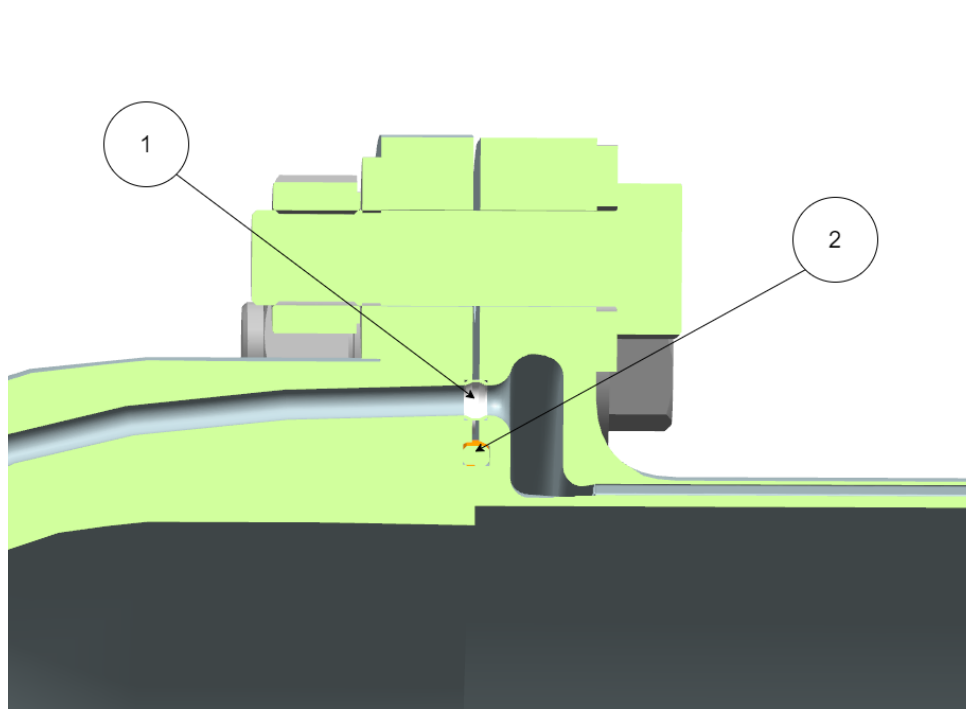Figure 3.28: Close-up of the bolted flanges

Figure 3.29: Bolted flange section, 1 - PTFE sealing ring for the oxidizer channels 2 - copper sealing

3.9 Test stand

In this final section I will present layout of the test stand for my design. My design consists of mounting plate, with holes for bolts, matching the ones in the engine flanges. The engine is attached via the flange and bolts to the mounting plane. Mounting plane is connected to the load cells, which are attached a steel beam construction. Due to the length and weight of the engine two supporting features are screwed into a plane on the construction in order to lower the bend load on the mounting plate, bolts and flange. The plane has to be movable, in the direction of the thrust, so the supports would not limit the thrust and compromise the tests. The oxidizer feeding system should include additional shut-off valves and pressure gages to asses the pressure in the piping and flow meter just before the oxidizer inlet. The whole oxidizer feed system should be tested before to adjust the feed pressure if need be, to more precisely determine the losses in the piping and cooling passages.
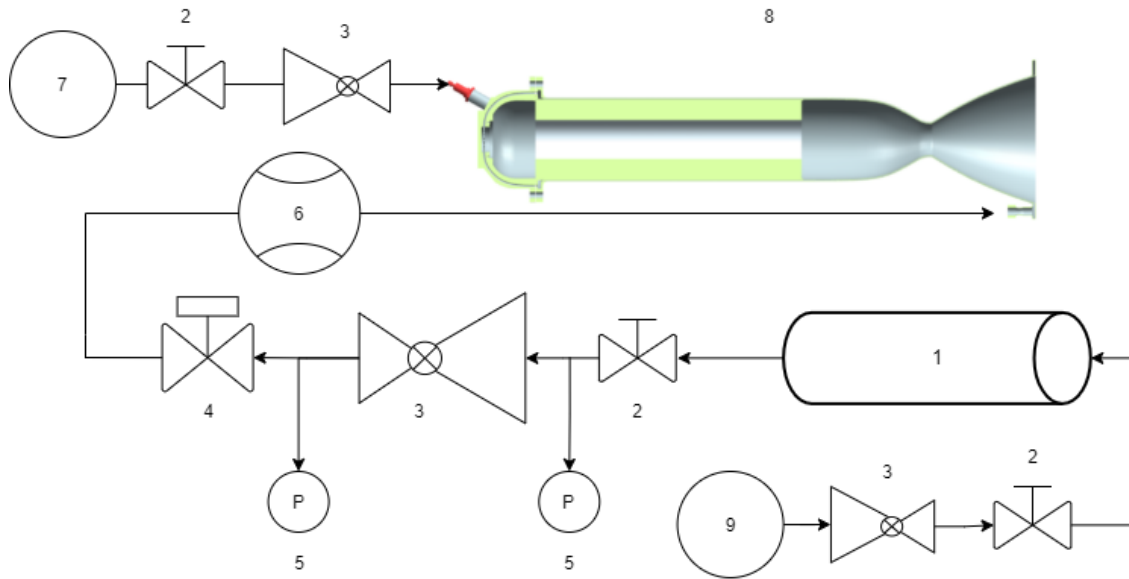
Figure 3.30: Feeding system diagram for testing 1 - Oxidizer tank, 2 - Shut-off valve, 3 - Pressure regulator, 4 - On-off valve, 5 - Pressure gage, 6 - Flowmeter, 7 - Gas supply for the igniter, 8 - Engine, 9 - Pressurant gas
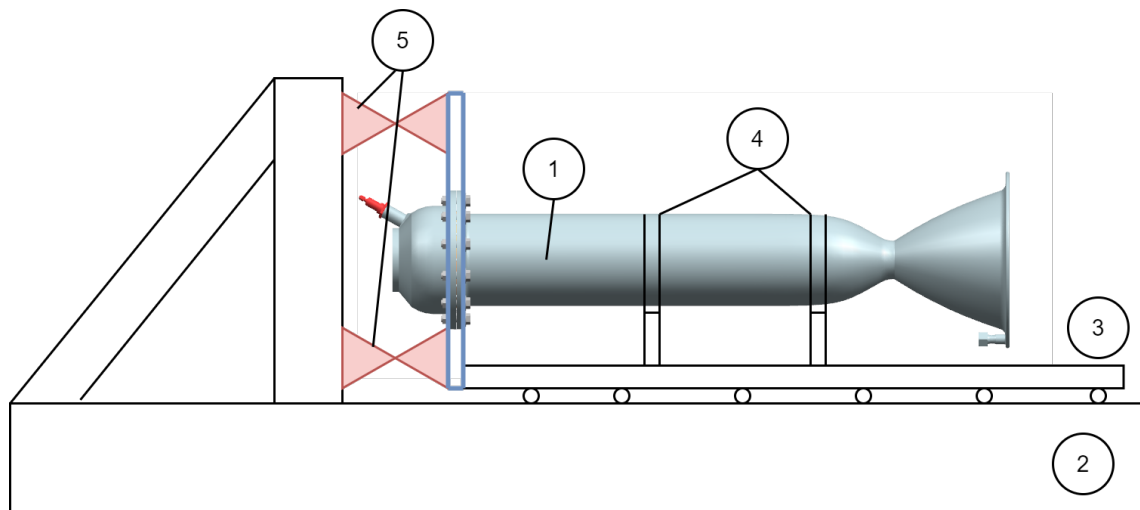

Figure 3.31: Schematics of the test stand, 1 - Engine, 2 - Beam construction, 3 Movable plane, 4 - Attachment rings, 5 - Loading cells

4. Conclusion

After the research regarding the hybrid rocket engines with emphases on their use as a propelling system for the sounding rockets I have conducted preliminary design of the propellant demands on such application with chosen propellant combination, liquid oxygen and paraffin wax. To further assess the suitable set-up for the vehicle feasibility analysis was conducted, resulting in choosing time of engine burn of 45 seconds. Based on my colleague's fuel grain design, which was designed for the same application, I have determined the dimensions, pressure and temperatures in the combustion chamber and nozzle. With the newly obtained data I have found the average thrust is greater compared to the values used in feasibility analysis. Based on the combustion pressure I have found the necessary wall thickness for the combustion chamber. The fabrication method for the nozzle is metal additive technology and material Inconel 625. For the oxidizer supply I have decided to use a gas pressure feed system, liquid oxygen serves as coolant and is fed into the channels in the nozzle wall at the nozzle exit plane. The design of the oxidizer and coolant systems offer a opportunity for a further investigation, flow modelling and experiments would help to get more precise design, but are beyond the scope of this thesis. For the ignitor I have adapted an approach, in which the ignition is initiated by a plasma torch, as a working fluid for the torch I have decided to utilize helium, serving as well as the pressurant gas. As a follow up research it would be desirable to investigate the possible weight savings, especially for the head casing, oxidizer flow, heat exchange between coolant, nozzle wall and combustion gasses and the limits in using the plasma torch as ignitor, where the length of the flame and would require experimental validation.

Bibliography

[1] David H. Huang Dieter K. Huzel. *Modern Engineering For Design Of Liquid-Propellant Rocket Engines.* 370 L'Enfant Promenade, SW, Washington, DC 20024: American Institute of Aeronautics and Astronautics, Inc., 1992.

[2] Ricardo Vieira Fernando de Souza Costa. "Preliminary Analysis of Hybrid Rockets for Launching Nanosats into LEO". In: (Oct. 2010). DOI: `10.1590/S1678-58782010000400012`.

[3] Oscar Biblarz George P. Sutton. *Rocket propulsion elements: An introduction to the engineering of rockets.* 111 River Street, Hoboken, NJ 07030-5774: John Wiley Sons, 2000.

[4] Joseph Gracy. *Restart Capabilities of Hybrid Rocket Motor Utilizing Gaseous Propane and Oxygen Injection System.* Mechanical Engineering Undergraduate Honors Theses. 2008.

[5] Kristoffer Hammargren. "Aerodynamics Modeling of Sounding Rockets: A Computational Fluid Dynamics Study". Master Level Thesis. Luleå University of Technology, 2014.

[6] Francesca Heeg et al. "Design and Test of a Student Hybrid Rocket Engine with an External Carbon Fiber Composite Structure". In: *Aerospace* 7.5 (2020). ISSN: 2226-4310. DOI: `10.3390/aerospace7050057`. URL: `https://www.mdpi.com/2226-4310/7/5/57`.

[7] Michael I. Judson Jr. "Direct Electrical Arc Ignition of Hybrid Rocket Motors". Graduate Thesis. Utah State University, 2015.

[8] Shinjae Kang et al. "Design and performance evaluation of hybrid rocket using 95 wt.% H2O2". In: (July 2016). DOI: `10.2514/6.2016-4864`.

[9] Michael Heard Katlin Davic Elizabeth Heard. *Experimental and Computational Investigation of a Dual-Bell Nozzle*. Tech. rep. Worcester Polytechnic Institue, 2014.

[10] Kenneth K. Kuo Martin J. Chiaverini. *Fundamentals of Hybrid Rocket Combustion and Propulsion*. 1801 Alexander Bell Drive, Reston, Virginia 20191-4344: American Institute of Aeronautics and Astronautics, Inc., 2006.

[11] G. Marxman and M. Gilbert. *Turbulent Boundary Layer Combustion in the Hybrid Rocket*. Tech. rep. Ninth Symposium (International) on Combustion, 1963.

[12] Ichiro Nakagawa. *Plasma torch igniter for hybrid rockets*. Tech. rep. Department of Aeronautics Astronautics, Tokai University, 2018.

[13] G. G. Uilliac and A. Karabeyoglo. *Hybrid Rocket Fuel Regression Rate Data and Modeling*. Tech. rep. American Institute of Aeronautics and Astronautics, 2006.